

**DUAL-GRADIENT DRILLING:  
INVESTIGATION OF TRANSIENT BEHAVIOR**

A Thesis

By

AARON JOHN MENDONSA

Submitted to the Office of Graduate and Professional Studies of  
Texas A&M University  
in partial fulfillment of the requirements for the degree of

MASTER OF SCIENCE

Chair of Committee,	Jerome Schubert
Committee Members,	Samuel Noynaert
	John Hurtado
Head of Department,	Daniel Hill

December 2016

Major Subject: Petroleum Engineering

Copyright 2016 Aaron Mendonsa

## ABSTRACT

As the industry seeks out exploration prospects in increasing water depths, the complexity of drilling in tight pore-pressure and fracture-pressure windows has become progressively more challenging. Conventional or single-gradient drilling has reached a physical limitation where the formation can no longer tolerate the hydrostatic pressure from a single column of drilling fluid. Narrow pressure windows require additional casing strings, which, when used with conventional drilling technology, complicates reaching geological targets.

There are numerous methods of dual-gradient drilling (DGD) – a subset of managed pressure drilling (MPD) – but each share the same principal. In each method, DGD seeks to eliminate the problems associated with water depth, as DGD closely matches the natural pressure gradient of the water depth. Dual-gradient refers to the ability to adjust two distinct fluid densities by controlling the annular pressure. Therefore, we can manage the effect of equivalent circulating density (ECD) in an effort to maintain bottomhole pressure (BHP) within a narrow operating window between pore pressure and fracture pressure. Therefore, DGD permits longer hole sections and less casing strings in comparison to conventional technology. In a sense, DGD allows development of wells that were at one time considered “*un-drillable*”.

We will focus on Statoil’s Controlled Mud Pressure field trial using Enhanced Drilling’s DGD technology (EC-Drill™) in the Troll field on the Norwegian Continental Shelf. The EC-Drill™ system is comprised of a subsea pump module (SPM) attached to a marine riser that pumps returns to a discrete mud return line. This system relies on a

partially evacuated riser made up of a blanket fluid of air and heavier drilling mud. The riser mud level can be influenced by adjusting the discharge pump rate of the SPM, that when run in automatic mode, the system will maintain constant bottomhole pressure. In contrast, the SPM can be operated in manual mode where a constant riser fluid level is maintained instead –termed ‘controlled mud level’ (CML).

The objective of this research study was to perform simulation on transient behavior during a connection break using Schlumberger software, Drillbench™. Connections made during conventional drilling are potentially precarious times to encounter well kicks due to the loss of annular friction, effectively reducing the BHP down to a static mud weight. In contrast, this research aims to highlight the efficacy of the EC-Drill™ system where the SPM remains circulating during connections, addressing both the U-tubing and loss of annular frictional pressure loss. The simulation software presented an in-depth understanding of the dynamic hydraulics with the capability of reproducing field trials with a level of accuracy that is not obtainable with other competitive steady-state models.

Results demonstrate that constant BHP can be simulated within a +/- 50-psi window, while responding to changes in drilling parameters and navigating tight formation/fracture gradient windows with a full-riser margin. This research required close collaboration with three primary partners – Statoil ASA®, AGR Enhanced Drilling®, and Schlumberger Ltd®.

## **DEDICATION**

*"A teacher affects eternity; He can never tell where his influence stops"*  
*-Henry Brooks Adams*

If one were to inspect my life and discover fleeting moments of accomplishment, it was because I stood on the shoulders of my teachers.

## **ACKNOWLEDGEMENTS**

I would like to thank my committee chair, Dr. Jerome Schubert for his guidance, support, and warmth throughout the course of my academics here at Texas A&M University. Unequivocally, I consider Dr. Schubert an integral mentor and person in my career and life.

Additionally, I would like to extend my gratitude to Dr. Samuel Noynaert and Dr. John Hurtado for their time, support, and openness throughout the course of this research.

None of this research would have been possible if not for Dr. John-Morten Godhavn from Statoil ASA who diligently guided me, supported my research interests, and was always there to answer questions.

I also want to extend my thanks to John Cohen with AGR Enhanced Drilling who sparked my interest in deepwater challenges.

Unbeknownst to Professor Fred Dupriest, he has inspired me immensely and re-ignited my passion for drilling. His teaching and mentorship has been invaluable.

Lastly, I want to thank Dr. Zhaoguang Yuan from Schlumberger. Dr. Yuan has consistently helped me throughout each phase of my simulation and has spent countless hours training, teaching, and helping me through this research. Truly, without him, none of this would be possible.

## TABLE OF CONTENTS

	Page
ABSTRACT .....	ii
DEDICATION .....	iv
ACKNOWLEDGEMENTS.....	v
TABLE OF CONTENTS.....	vi
LIST OF FIGURES .....	ix
LIST OF TABLES .....	xii
1. INTRODUCTION AND LITERATURE REVIEW .....	1
1.1 Managed Pressure Drilling.....	3
1.1.1 Equivalent Circulating Density.....	3
1.1.2 Pore Pressure and Fracture Pressure .....	5
1.1.3 Constant Bottomhole Pressure .....	7
1.1.4 Dual-Gradient Drilling (DGD).....	9
1.2 EC-Drill™ Technology .....	16
1.2.1 System Fundamentals .....	17
1.2.2 Field Testing and Operation .....	24
1.3 Well Control Issues.....	26
1.3.1 Well Influxes.....	26
1.3.2 Lost Circulation .....	28
2. METHODOLOGY.....	31
2.1 Initial Planned Case Study .....	32
2.2 Revised Case Study .....	33
2.3 Software .....	34
2.3.1 Possible Options .....	34
2.3.2 Software Version .....	35
3. SIMULATION DESIGN.....	36
3.1 Basic Input.....	36
3.1.1 Summary .....	37

3.1.2	Description.....	37
3.1.3	Survey.....	38
3.1.4	Formation.....	39
3.1.5	Pore Pressure and Fracture Pressure .....	40
3.1.6	Wellbore Geometry .....	41
3.1.7	Drillstring.....	44
3.1.8	Drilling Fluid.....	46
3.1.9	Temperature.....	47
3.2	Expert Input.....	48
3.2.1	Model Parameters.....	48
3.2.2	Eccentricity .....	49
3.2.3	Surface Pipeline.....	49
3.2.4	RCH and Choke .....	49
3.2.5	Dual Gradient Mode with Subsea Pump .....	49
3.3	Run Configuration.....	51
3.3.1	Batch Configuration .....	51
4.	RESULTS AND DISCUSSION.....	54
4.1	Mud Level .....	54
4.2	Rig Pump Pressure .....	56
4.3	Rig Pump Rate .....	57
4.4	Subsea Pump Module Pressure.....	58
4.5	Subsea Pump Module Rate.....	59
4.6	Bottomhole ECD.....	61
4.7	ECD Profile .....	62
4.8	Bottomhole Pressure .....	63
4.9	Well Pressure Profile .....	64
4.10	Mud Flowrate .....	65
4.11	Bottomhole Temperature .....	66
4.12	Temperature Profile.....	67
4.13	Pit Gain .....	68
4.14	Pressure Drop across Bit.....	69
4.15	Pumped Volume .....	70
4.16	Equivalent Viscosity .....	71
4.17	Reynolds Number Profile.....	72
4.18	Friction Pressure Loss Gradient.....	73
5.	LIMITATIONS AND DEVELOPMENT.....	75
6.	CONCLUSIONS.....	77
	NOMENCLATURE.....	79

REFERENCES ..... 82

SUPPLEMENTAL SOURCES CONSULTED ..... 84

APPENDIX A ..... 85

APPENDIX B ..... 95

## LIST OF FIGURES

	Page
Figure 1 - The Relationship Between Annular Frictional Pressure Loss and Static Mud Weight.....	4
Figure 2 - Deepwater Conditions Require Additional Casing Strings Due to Narrow Window .....	6
Figure 3 - Conventional Drilling W/ Typical Well Issues Seen With ECD.....	7
Figure 4 - Constant Bottomhole Pressure Drilling.....	8
Figure 5 - Illustration Of DGD "Margin" in Red Shows That Calculating From Seafloor Allows a Larger Drilling Window.....	10
Figure 6 - DGD PP And FP Are Widened Significantly From Conventional Pressure Gradients (Relative to the Seafloor) .....	11
Figure 7 - Deepwater Environments Tend to Have a Narrower Drilling Window Due to a Lower Overburden (Axon Energy, 'Navigating Narrow Drilling Margins', 2015) .....	12
Figure 8 - Conventional Circulation and SMD Circulation Using an RCD and MLP (Axon Energy, 'Navigating Narrow Drilling Margins, 2015) .....	13
Figure 9 - Same Bottomhole Pressure Is Felt at Formation With Less Mudline Pressure Felt With DGD (Chevron, 2014) .....	14
Figure 10 - CML System Configurations (Stave. R, May 2014).....	18
Figure 11 - An Increase in Flow Velocity or KE Must Correspond to a Decrease in PE and Internal Pressure in Order for the Conservation of Energy to Hold True (Nave. C, 2012) .....	20
Figure 12 - CML System Schematic (Cohen. J, Stave. R, et al. May 2014) .....	22
Figure 13 - Subsea Pump Module Head Curves (Cohen. J, Stave. R, et al. May 2014).....	23
Figure 14 - EC Drill SPM (Left) and Running Riser With SPM Attached (Right) .....	25

Figure 15 - EC- Drill SPM in Moonpool Attached to Drilling Riser (Enhanced Drilling, 2014) .....	25
Figure 16 - Graphical Display of a Well Kick Where Both Annulus and Drill Pipe Show Differential Needed to Balance Hydrostatic and Formation Pressure (Drilling Handbook) .....	28
Figure 17 - Breakout Occurs in the Direction of $H_{min}$ While Lost Returns Occur in the Direction of $H_{max}$ (British Geological Survey).....	29
Figure 18 - Graphical Display of Given Case where SPM at 1135', WD at 6000', TD at 26800' (Enhanced Drilling) .....	31
Figure 19 - Auto-Completed Summary Input .....	37
Figure 20 - Description Input .....	38
Figure 21 - Survey Input With MD, Inclination and Azimuth .....	39
Figure 22 - Geology and Thermophysical Properties .....	40
Figure 23 - Pore Pressure and Fracture Pressure Window .....	41
Figure 24 - Wellbore Geometry .....	42
Figure 25 - Wellbore Schematic With Casing Strings.....	43
Figure 26 - Drillstring, BHA, and Bit Configuration .....	44
Figure 27 - BHA Configuration (Statoil and Schlumberger) .....	45
Figure 28 - Mud Properties.....	46
Figure 29 - Temperature Model .....	47
Figure 30 - Mud Level During Connection for Drillstring and Riser .....	55
Figure 31 - Ramping of Rig Pumps During a Connection .....	56
Figure 32 - Rig Pump Rate During Connection .....	57
Figure 33 - Boundary Pressure at 1135' During Connection .....	58
Figure 34 - Unfiltered Subsea Pump Rate .....	59
Figure 35 - Filtered Subsea Pump Rate.....	60

Figure 36 - Bottomhole Equivalent Circulating Density During Connection.....	61
Figure 37 - Equivalent Circulating Density Profile by Depth.....	62
Figure 38 - Bottomhole Pressure During Connection.....	63
Figure 39 - Well Pressure Profile by Depth.....	64
Figure 40 - Mud Flowrate In and Out.....	65
Figure 41 - Bottomhole Temperature at 26,800' During Connection.....	66
Figure 42 - Temperature Profile by Depth .....	67
Figure 43 - Pit Gain Measured in Barrels .....	68
Figure 44 - Pressure Loss across Bit in Psi.....	69
Figure 45 - Pumped Volume Measured in Bbls .....	70
Figure 46 - Equivalent Viscosity Profile by Depth.....	71
Figure 47 - Reynolds Number Profile by Depth .....	72
Figure 48 - Frictional Pressure Loss Gradient by Depth .....	73

## LIST OF TABLES

	Page
Table 1 - Batch Configuration Run .....	53
Table 2 - Sensor Offset From Bit (Statoil ASA).....	95
Table 3 - Stabilizer Summary (Statoil ASA).....	96
Table 4 - BHA Nozzle Summary (Statoil ASA).....	96
Table 5 - BHA Specification Sheet (Statoil ASA) .....	97

## **1. INTRODUCTION AND LITERATURE REVIEW**

The frontiers of deepwater drilling are continuously extended as exploratory wells are discovered in greater water depths. To no avail, the industry initially attempted to adapt operational and engineering practices from shallow wells to deepwater. To overcome the deepwater challenges, operators were forced to push beyond conventional limits in terms of both technology and design criteria.

There are a number of challenges that have the potential to severely complicate reaching desired geological targets. For example, low overburden stress to a large water column results in a low stress regime. As a result, weak and unconsolidated sediments pose impending geo-hazards to well objectives. Additionally, asymmetrical topography, abnormally pressured formations, and erosive soil conditions all require precise engineering mitigation.

Increasing the water depth effectively reduces the total overburden gradient, which coincidentally reduces the fracture gradient. Therefore, as a function of water depth, the drilling window between pore pressure and fracture pressure will decline. This small operational window necessitates an increase in the number of casing strings and smaller production tubing at total depth. In terms of well control, the prospect of fracturing a formation and inducing losses are higher in deepwater wells.

As mentioned above, due to low overburden, wellbore instability issues require higher mud weights in order to prevent hole collapse. Well geometry and well trajectory must consequently include an understanding of the stress regime to minimize borehole enlargement or conversely, collapse. Extended reach wells exhibit

an amplified response where both formation fracture due to annular frictional loss, and borehole instability are more likely to occur at higher inclination.

Managed Pressure Drilling (MPD) is a dynamic response to management of small operating drilling windows through adaptive and deliberate control of circulating density. MPD has proven to be effective in addressing narrow pressure windows, lost circulation issues, and well influxes. This thesis will seek to introduce the fundamentals of MPD as well as highlight the applications of dual-gradient drilling technology.

(Rocha, Arduino, et al. 2003)

## 1.1 Managed Pressure Drilling

As a result of non-productive time (NPT), high costs were the principal driver in MPD development. Objectives included minimizing NPT due to wellbore pressure issues, limiting lost circulation, increasing rate of penetration (ROP) and extending casing string depths. All of these objectives are achieved through diverse methods of MPD, but each method shares the same fundamentals. Unvaryingly, the drilling process must be able to “...precisely control the annular pressure profile throughout the wellbore. The objectives are to ascertain the downhole pressure environment limits and to manage the annular hydraulic pressure accordingly.” (IADC Subcommittee 2011) In summary, MPD must be able to adapt to changes in wellbore conditions dynamically.

### 1.1.1 Equivalent Circulating Density

To understand the relevance of this research, it is important to highlight the fundamentals of annular frictional pressure loss. We start with the basic expression for the total pressure loss or pump pressure ( $\Delta P_P$ ):

$$\Delta P_P = \Delta P_{DS} + \Delta P_{Bit} + \Delta P_A + \Delta P_i$$

where  $\Delta P_{DS}$  denotes the pressure loss from the drillstring,  $\Delta P_{Bit}$  denotes the pressure loss from the bit,  $\Delta P_A$  represents the frictional pressure loss from the annulus, and lastly,  $\Delta P_i$  signifies any initial pressure loss of the system, perhaps static. We can calculate equivalent circulating density once we evaluate the following:

1. Fluid Velocity ( $V$ ) –resulting from flow rate and geometry
2. Mud Rheology ( $\rho$ ) –derived from rotational viscometer readings
3. Reynolds Number ( $N_{Re}$ ) –where  $Re > 2300$  is considered laminar

4. Friction factor –from API 13D can be calculated using  $f = 24/N_{Re}$

Once the above expressions are computed, we can evaluate the individual pressure losses per unit length:

$$\frac{\Delta P_A}{\Delta L} = \frac{f V^2 \rho}{25.81 (D_2 - D_1)}$$

Using the expression above, we can then evaluate the annular frictional pressure loss (AFP) that is specific to the frictional pressure that occurs in the annulus while circulating.

$$ECD [ppg] = ESD [initial\ mud\ weight] + \frac{\Delta P_A}{0.052 (True\ Vertical\ Depth)}$$

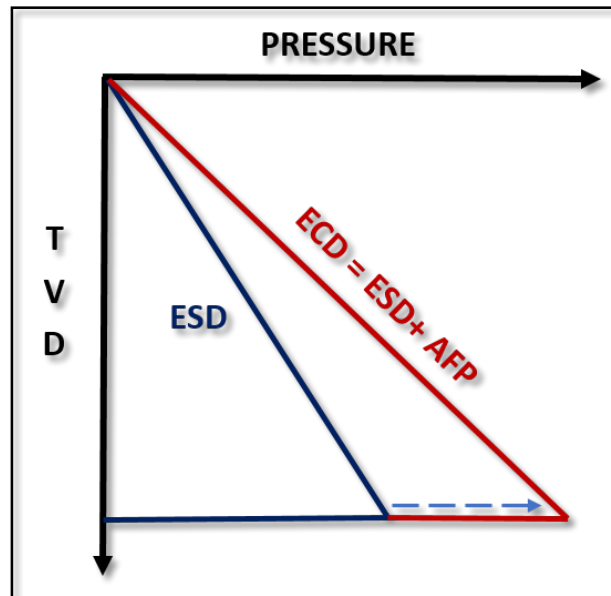


**Figure 1 - The Relationship Between Annular Frictional Pressure Loss and Static Mud Weight**

We observe from **Figure 1** and the expression above that ECD can be discretely categorized as hydrostatic head with the addition of annular friction (AFP) and cuttings loading. (Rehm. B, Schubert. J, et al. *Managed Pressure Drilling*, 2008)

### **1.1.2 Pore Pressure and Fracture Pressure**

In 1943, Karl von Terzaghi, known as the “father of soil mechanics”, published a fundamental principle in *Theoretical Soil Mechanics*. Terzaghi defined effective stress in relation to both pore pressure and total stress as a function of compaction. The expression below signifies that as rocks are compacted, the fluids within the pore spaces, under stress, depart. The pore volume or porosity ultimately lessens due to compaction and effective stress consequently rises. We observe that the total stress is equal to the sum of effective stress (grain-to-grain) and pore pressure.

$$\sigma_{total\ stress} = \sigma_{effective} + P_{pore}$$

or rearranged:

$$\sigma_{effective} = \sigma_{total\ stress} - P_{pore}$$

In deepwater, abnormal pore pressures are a critical concern to well operations. We observe from the above relations, that as the pore pressure increases abnormally for a given total stress, the total grain-to-grain effective stress declines. On land, we generally observe that as formation depth increases, fracture pressure also increases due to an increase in sediment overburden.

This relationship does not remain true in deepwater environments. In contrast, formation strength is lower as the increasing overburden now comprises of seawater rather than rock. Therefore, drilling operations must constantly be aware of potential convergence between mud weight and fracture pressure throughout each interval. Conventionally, in order to address this declining drilling window, the number of casing strings would need to be substantial to reach the desired total depth. This is due to the convergence between the chosen mud gradient and the pore pressure at shallow

depths, therefore requiring casing strings at smaller intervals than on land operations (Andriessse, D. *Effect of Abnormal Pore Pressure on Deep Water Drilling*, 1976). We observe this relationship in **Figure 2**.

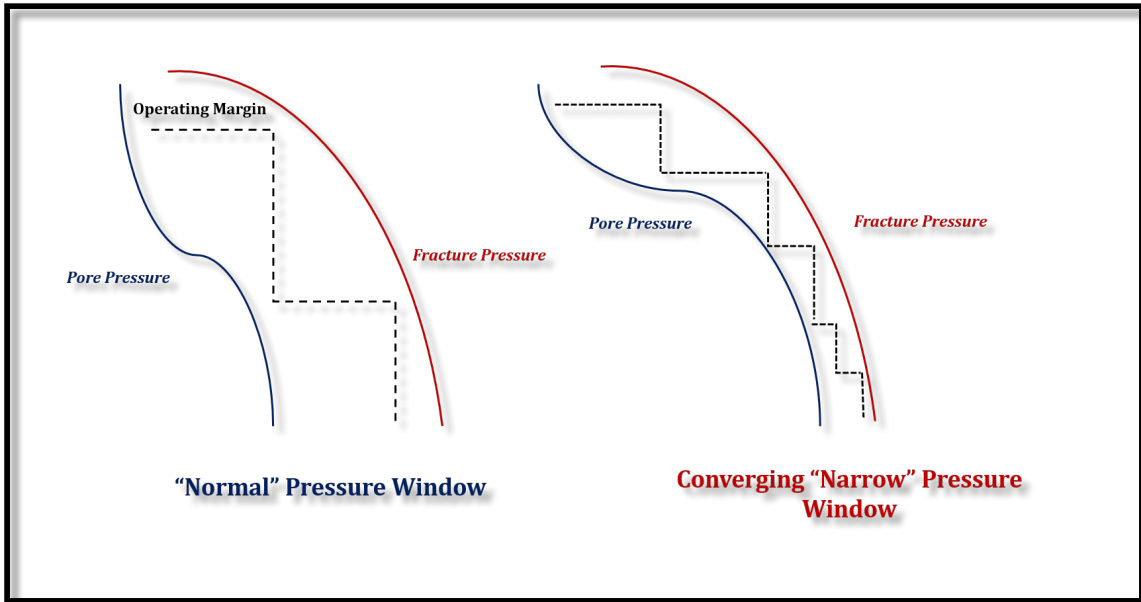


**Figure 2 - Deepwater Conditions Require Additional Casing Strings Due to Narrow Window**

The above figure illustrates the difficulty of drilling deepwater due to both imperfect prediction of pore pressures and formation strength and a continuously narrow margin. Both subject well operations to the possibility of either a well control issue or lost circulation. This thesis will endeavor to demonstrate the applicability of dual-gradient drilling in addressing these specific challenges.

### 1.1.3 Constant Bottomhole Pressure

CBP or *constant bottomhole pressure* is a subclass of managed pressure drilling. This respective type of process maintains a constant annular pressure despite rig pump operations –circulating, tripping, and pumps off. Different formation zone intervals dictate the tolerance of the annular pressure range, allowing drilling to continue despite dynamic changes in pore pressure and fracture pressure. CBP addresses the conventional problem with heterogeneous strength rock where ECD is acceptable within one zone but risks fracture and losses within another zonal interest. We observe the distinctive advantage between conventional drilling practices and CBP drilling in **Figures 3 and 4**.

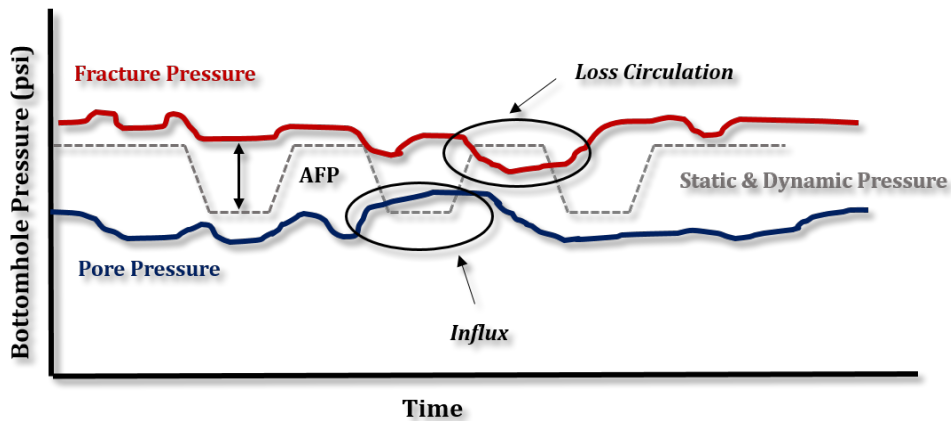


**Figure 3 - Conventional Drilling W/ Typical Well Issues Seen With ECD**

We observe from the above figure that navigating the pore/fracture pressure window is challenging and poses significant risk of either influx or lost circulation, or both. With CBP, shown in **Figure 4**, we maintain a static bottomhole pressure by

adjusting the choke/annular backpressure. (Vieira. P, et al. *Constant Bottomhole Pressure*, 2008)

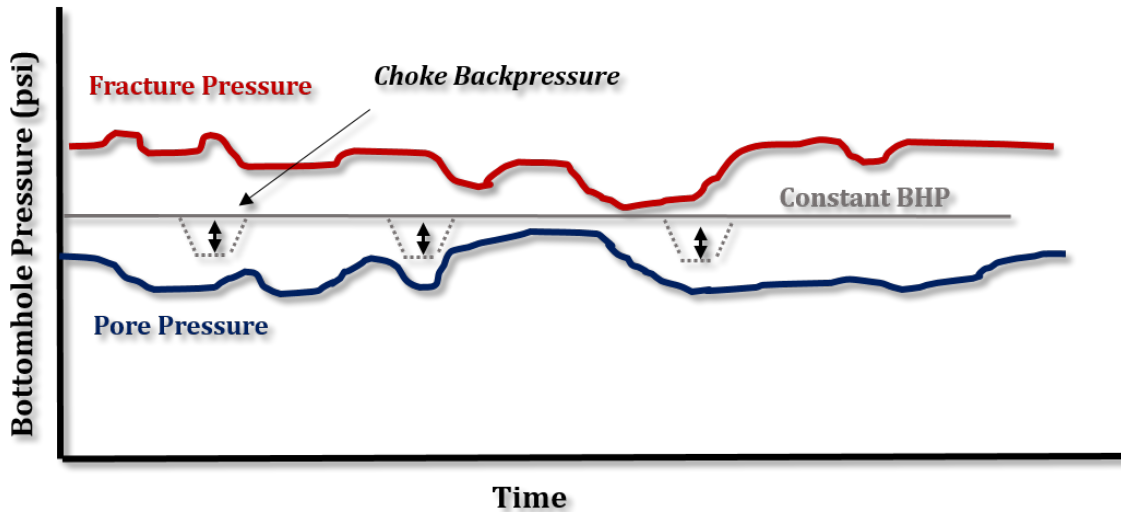


Figure 4 - Constant Bottomhole Pressure Drilling

From the prior sections, we summarize the following:

- *Fundamentals of annular pressure loss (ECD)*
- *Differences between overburden in offshore operations*
- *Challenges with navigating pore/fracture pressure windows with ECD*
- *Advantages of constant bottomhole pressure*
- *Addressing tight windows with MPD*

A significant amount of well-bore instability, lost circulation, and differential sticking issues occur due to geological uncertainty. Although current models are improving both the estimation of pore and fracture pressure below the mudline in deepwater, geologic abnormalities, transition zones, and subnormal pressured

formations prove challenging to conventional drilling operations. MPD or explicitly, dual-gradient drilling, could prove a viable solution with its high adaptability to dynamic wellbore conditions. (Rehm, B, Schubert, J, et al. *Managed Pressure Drilling*, 2008)

#### **1.1.4 Dual-Gradient Drilling (DGD)**

Dual-gradient drilling (DGD) has had limited commercial success due to the required high initial capital expenditure, unwanted risk in a low commodity price environment, and complexity involved with operation. However, due to the limitations encountered with conventional drilling, DGD has become progressively more researched and field-tested in order to reach geologic targets that were, at one time, considered technologically or economically unviable.

The fundamentals of DGD are quite simple to understand if one understands the primary difference in how each pressure gradient is calculated. In conventional riser drilling, all the pressure gradients are calculated with reference to the rotary kelly bushing (RKB). This differs from DGD in which the pressure gradient is calculated with respect to the seafloor mudline (ML). DGD effectively “widens” the pore/fracture pressure window, allowing both a reduction in casing strings needed, but also, larger production tubing in the pay zone. This advantage is primarily gained from the fact that the pore and fracture gradients are now relative to the seafloor, and not the RKB.

In this section, we will focus on the mud-lift principle (SMD), which illustrates dual-gradient drilling in the clearest fashion. Later, we will discuss a

variation of this technology, namely CML/CMP, from which this thesis investigates transient behavior. Despite different implementations, the fundamental principles remain the same as both DGD technologies attempt to closely match the seawater gradient above the ML.

**Figures 5 & 6** show the comparison between DGD pore/fracture gradients calculated with reference to the ML and pore/fracture gradients calculated with reference to the RKB. Relating the gradients with respect to the seafloor allows a wider drilling window in which to not only operate, but also operate with a kick margin.

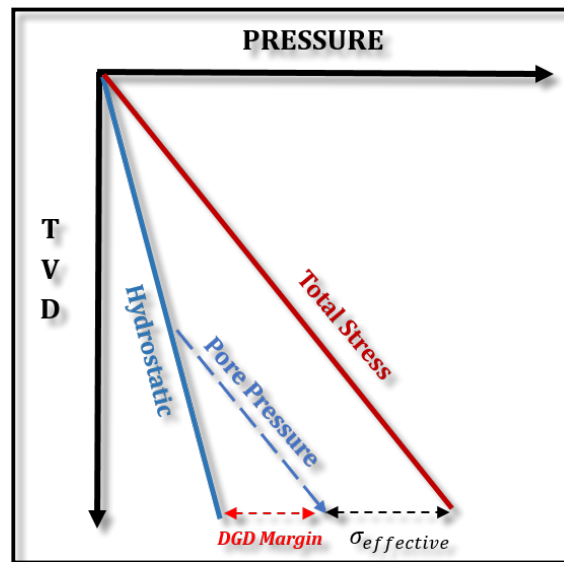


**Figure 5 - Illustration Of DGD "Margin" in Red Shows That Calculating From Seafloor Allows a Larger Drilling Window**

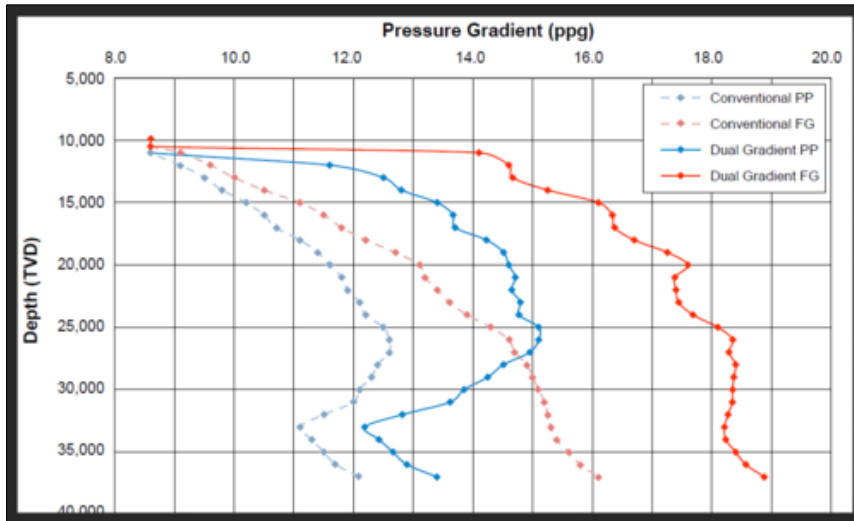


**Figure 6 - DGD PP And FP Are Widened Significantly From Conventional Pressure Gradients  
(Relative to the Seafloor)**

The term *dual-gradient* denotes two discrete fluids, each offering a variation in both density and hydrostatic pressure to each other respectively. In the case of subsea mud-lift drilling, the fluids comprise of seawater and drilling mud in the annulus. A mudline pump is used to pump the lighter fluid returns up to the surface. The seafloor pump has an intake pressure that is lighter than traditional mud and therefore is equivalent to the seawater hydrostatic pressure. To the wellbore, a higher density mud is felt at a lower vertical depth to address formation and pore pressure. **Figure 7** demonstrates the trend we observe in deepwater while **Figure 8** illustrates the fundamentals of SMD, noting the lower pressure felt at the mudline.

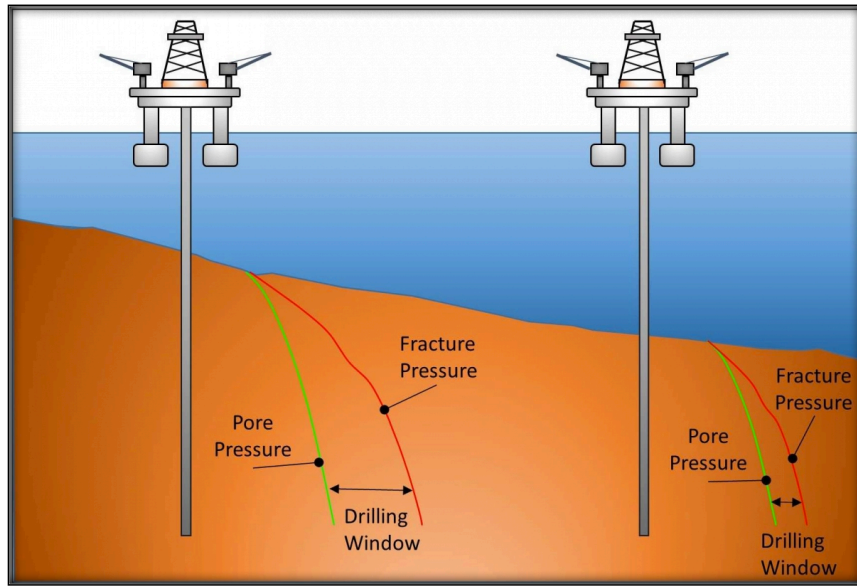


**Figure 7 - Deepwater Environments Tend to Have a Narrower Drilling Window Due to a Lower Overburden (Axon Energy, 'Navigating Narrow Drilling Margins', 2015)**

As we observe from **Figure 8**, the riser is filled with a lower density fluid with a density close to seawater, which attempts to closely match the conditions of natural conditions of seawater hydrostatic. The riser and wellbore are isolated with a rotating diverter (RCD), which forms a mechanical seal between the two fluids. Below the RCD, the wellbore is filled with high density drilling mud that is circulated through the annulus, and pumped up the mud return line (MRL) with the mud lift pump (MLP).

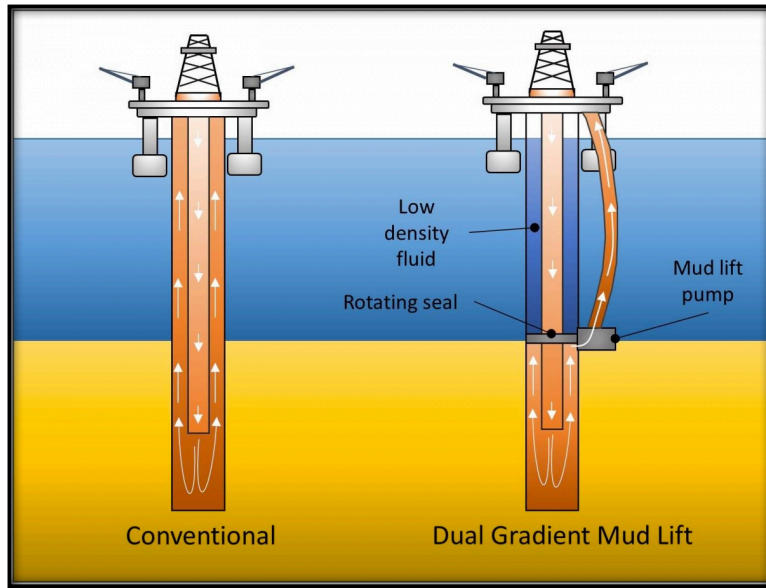


**Figure 8 – Conventional Circulation and SMD Circulation Using an RCD and MLP (Axon Energy, ‘Navigating Narrow Drilling Margins, 2015)**

For example, if we were to drill at 10,000 feet conventionally with a mud weight (MW) of 13.5 pounds per gallon (ppg), the hydrostatic pressure at the seafloor would be approximately 7,020 psi. Conversely, if we drill the same condition of 10,000 feet water depth using DGD, the seafloor pressure would be around 4450 psi with the density of seawater at 8.55 ppg. To be specific, the same bottomhole pressure is felt in both processes, only requirement of DGD, is that higher mud weight is used due to the lower vertical depth. We can observe this scenario in **Figure 9** – which demonstrates the ability to mimic natural conditions of deepwater reservoirs.

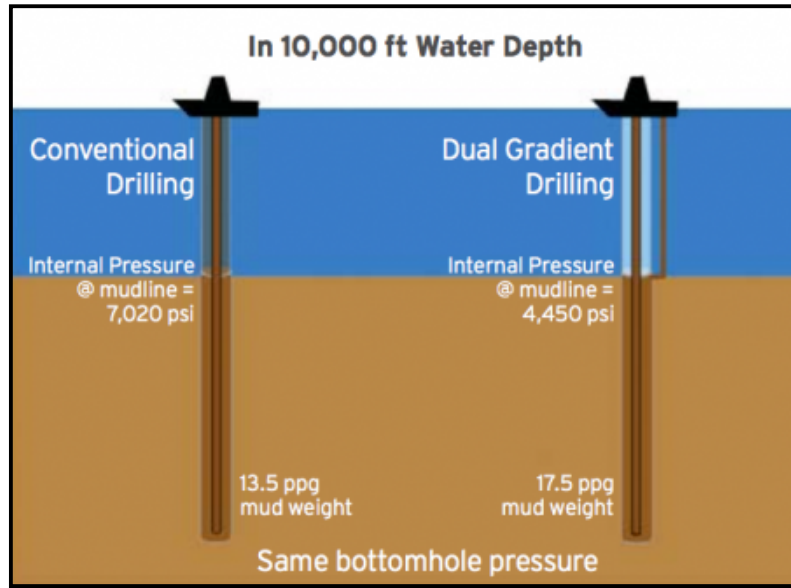


**Figure 9 - Same Bottomhole Pressure Is Felt at Formation With Less Mudline Pressure Felt With DGD (Chevron, 2014)**

In order to demonstrate to the reader, the efficacy of DGD, it is important to show the hydraulic system equations. There are three primary systems we need to consider:

- Riser to seafloor pressure
- Subsea pump module differential
- Below mudline (BML) wellbore pressure profile

We describe system 1 as the water depth hydrostatic pressure or equivalently, the inlet pressure of the subsea pump module:

$$p_{seafloor} = p_{outlet} = 0.052\rho_{seawater}D_{water}$$

For system 2, the subsea pump module, the differential across the subsea pump module can be described as the difference between the outlet and inlet pressure.

$$\Delta p_{spm} = p_{outlet} - p_{intake}$$

We can further describe  $\Delta p_{spm}$ , the differential across the subsea pump module with regards to water depth,  $D_{water}$ :

$$\Delta p_{spm} = 0.052\rho_m D_{water} + \Delta p_{f,return\ line} - 0.052\rho_{seawater} D_{water}$$

$$\Delta p_{spm} = 0.052(\rho_m - \rho_{seawater}) D_{water} + \Delta p_{f,return\ line}$$

Following system 2, we now consider system 3, where we designate the mud weight needed  $\rho_m$  and the bottomhole pressure as  $p_{bhp}$ . Understanding that the sum of pressures from system 1 to 3 is equal to the bottomhole pressure, we describe  $p_{bhp}$  as:

$$p_{bhp} = p_i + 0.052\rho_m D_{BML}$$

where we define:

$$p_i = 0.052\rho_{seawater} D_{water}$$

Rearranging to solve for mud weight:

$$\rho_m = \frac{p_{bhp} - p_i}{0.052 * D_{BML}}$$

Once we determine the required mud weight, we can then describe the wellbore pressure profile as  $p$ :

$$p = p_i + 0.052\rho_m(D - D_{water}) + \Delta p_{f,annulus}$$

where  $\Delta p_{f,annulus}$  represents the annular frictional loss that was described earlier as ECD. (Choe. J, Schubert. J, et al., December 2007)

We summarize the hydraulic equations below for both the static and dynamic pressures (Sharifur. R, Dowell. D, et al., SPE-174881, September 2015):

- $BHP_{\text{STATIC}} = \text{Mud line pump (MLP) inlet pressure} + \text{Hydrostatic pressure below MLP}$
- $BHP_{\text{DYNAMIC}} = \text{MLP inlet pressure} + \text{Hydrostatic pressure below MLP} + \text{AFP}$

## 1.2 EC-Drill™ Technology

In this thesis we are going to examine a specific DGD/MPD system engineered by Enhanced Drilling™, namely the EC Managed Pressure Drilling system. The EC Drill™ technology enables operators to adjust annular mud height in order to reach complex geological targets. The ability to adapt BHP to dynamic drilling conditions, otherwise known as *controlled mud level* or CML, has numerous advantages over conventional systems. Reported benefits include:

1. Drilling narrow pore/fracture pressure windows
2. Real-time BHP and mud level control
3. Early gain and loss detection abilities
4. ECD management during transient events

Fundamentally, the system relies on a subsea pump module (SPM) attached to the riser at a specific depth. The SPM acts as a drainage pump where the fluid level in the riser can be adjusted by increasing or decreasing the pump speed, directly changing BHP accordingly. (Enhanced Drilling, *EC-Drill™ Capability*, 2016)

This respective technology, due to its adaptive abilities, can drill the following two categories of wells with no equipment modifications needed (Rajabi.M, Stave. R, et al. SPE-151100, June 2012):

- *Conventional wells* –A full riser or a full hydrostatic column of conventional drilling mud does not exceed formation strength
- *Special wells* –the formation strength will be exceeded by a full riser and therefore, it requires drilling that matches the natural pressure gradients of formations. Adjustments will be made to both the riser fluid height and mud density.

### **1.2.1 System Fundamentals**

Earlier, we discussed the fundamental hydraulics and concept of DGD systems where the wellbore consists of a heavy drilling mud while the riser is filled with a lighter blanket fluid. The CML system is a simpler variation of DGD as there consists of only a single gradient fluid, conventional mud, in both the wellbore and riser.

BHP is controlled using a subsea pump attached to a riser where the riser is partially evacuated with air. During transient events such as connections, the riser level is filled higher, once circulation stops, accounting for the loss of AFP. Conversely, once the connection is made and circulation starts, the riser level drops to account for the additional AFP. The typical configuration for the CML system is as follows and corresponds to **Figure 10**:

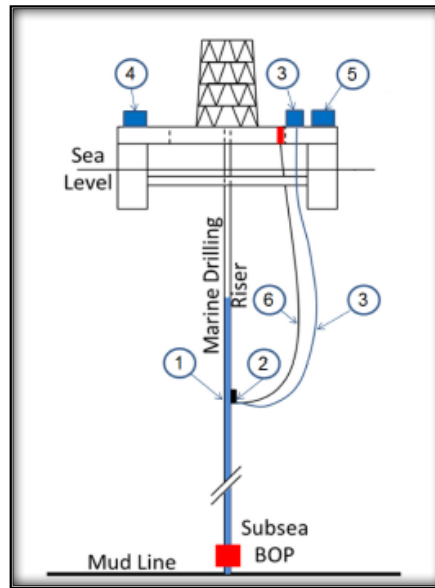


**Figure 10 - CML System Configurations (Stave. R, May 2014)**

Where we denote the following components that correspond to the above figure:

- Modified riser joint (MRJ)
- Subsea pump module (SPM)
- Umbilical for hydraulics and power
- Office and tool container
- Power and control system container
- Mud return line (MRL)

The SPM is attached to the riser traditionally between 1000 – 1200 feet where the riser is partially evacuated with air. As mentioned above, the SPM acts as drainage pump where pump power is chosen by determination of the pressure differential and desired flow rate requirements. (Stave. R, May 2014)

We will discuss in the interest of thoroughness both the fundamentals of pump pressure and flow rate through the use of Bernoulli's equation while additionally demonstrating the specifics of the pump used in EC-Drill™. Bernoulli's equation is a seminal expression for the conservation of energy with respect to fluid flow. We will demonstrate step-by-step the relationship between pressure and flow rate below (assuming steady-state):

$$\mathbf{Pressure} = \frac{\mathbf{Force}}{\mathbf{Area}} = \frac{\mathbf{Force} \times \mathbf{distance}}{\mathbf{Area} \times \mathbf{distance}} = \frac{\mathbf{Work}}{\mathbf{Volume}} = \frac{\mathbf{Energy}}{\mathbf{Volume}}$$

$$PE_{inlet} + KE_{inlet} = PE_{outlet} + KE_{outlet}$$

$$P_i + \frac{1}{2}\rho v_i^2 + \rho g h_i = P_o + \frac{1}{2}\rho v_o^2 + \rho g h_o$$

where  $P_i$  and  $P_o$  denote pressure energy per unit volume,  $\frac{1}{2}\rho v_i^2$  and  $\frac{1}{2}\rho v_o^2$  denote kinetic energy per unit volume and  $\rho g h_i$  and  $\rho g h_o$  denote potential energy per unit volume.

As we see above, Bernoulli's principle is the conservation of fluid flow energy, discretized by the sum of initial static pressure, potential energy, and kinetic energy. The above expression implies that an increase in the speed of a fluid or velocity, the same as stating an increase in kinetic energy, equally corresponds to a decrease in potential energy and static internal energy. We can see this phenomenon in **Figure 11** below, where with all things being equal, to have the same volumetric flow rate, the flow velocity must increase, and therefore, the static pressure must correspondingly decrease (Nave. C, 2012).

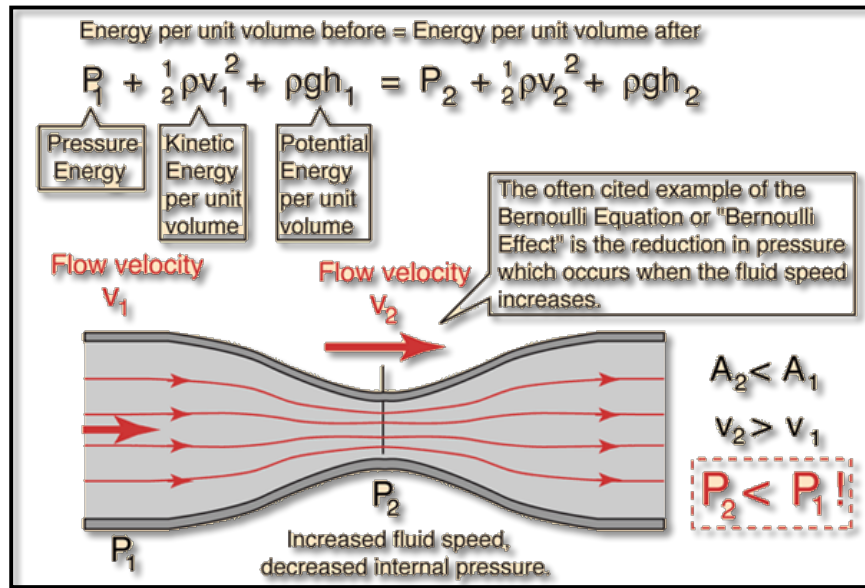


**Figure 11 - An Increase in Flow Velocity or KE Must Correspond to a Decrease in PE and Internal Pressure in Order for the Conservation of Energy to Hold True (Nave. C, 2012)**

In logical succession we have explained the fundamental principles behind work per unit volume or pressure. However, we would be remiss without briefly examining the basics of a single pump.

We recall the affinity laws that determine pump selection for a given system pressure at a chosen flow rate:

1<sup>st</sup> Affinity Law

$$\frac{Q_1}{Q_2} = \frac{N_1}{N_2}$$

The first affinity law states that flow rate is proportional to shaft speed where  $Q_N$  denotes volumetric flow rate and  $N_N$  denotes shaft speed in RPM.

## 2<sup>nd</sup> Affinity Law

$$\frac{P_1}{P_2} = \left(\frac{N_1}{N_2}\right)^2$$

The second affinity law states that pressure is proportional to the square of the shaft speed where  $P_N$  represents pressure or head (psi or feet) and  $N_N$  represents shaft speed in RPM.

Using an iterative process, we can determine the pump power needed in order to overcome system pressure at a given flow rate.

$$Power \text{ (Watts or HP)} = \frac{\rho P Q g}{\eta}$$

where  $\rho$  denotes fluid density,  $P$  denotes pressure,  $Q$  as flow rate,  $g$  as the gravitational constant, and lastly  $\eta$  as pump efficiency.

We can see from the above expression that for a given system pressure head at a chosen flow rate and accounting for pump efficiency, we can compute the pump power requirements. (Milnes. M, January 2007). Subsequently, we will now illustrate the CML subsea pump model with specifications.

We show in **Figure 12** the schematic of the CML system where the subsea pump returns both cuttings and drilling fluid via a mud return line. The SPM is a variation of a centrifugal pump where in contrast to traditional impellers, rotating disks are used to discharge.

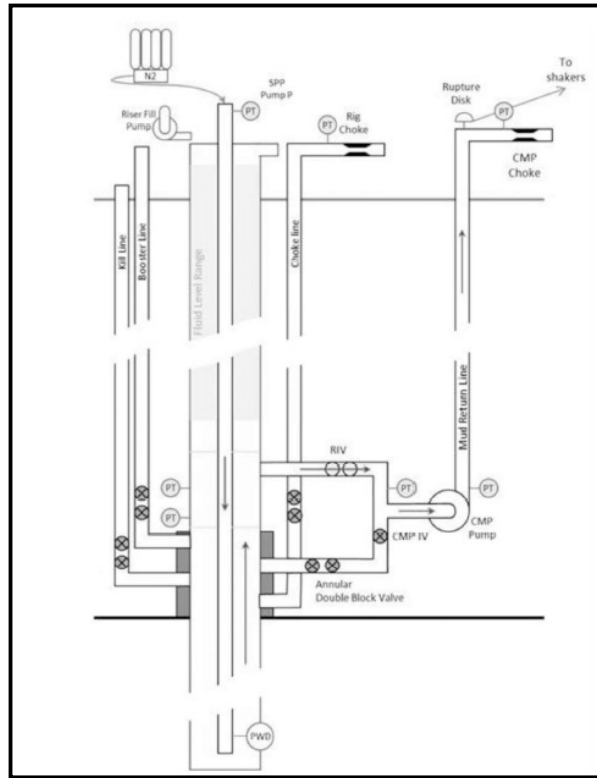


**Figure 12 - CML System Schematic (Cohen. J, Stave. R, et al. May 2014)**

Recalling the pump affinity laws mentioned above, we similarly show in **Figure 13**, the SPM model head curves where for a given volumetric flow rate and a desired shaft speed, total pressure head can be determined.

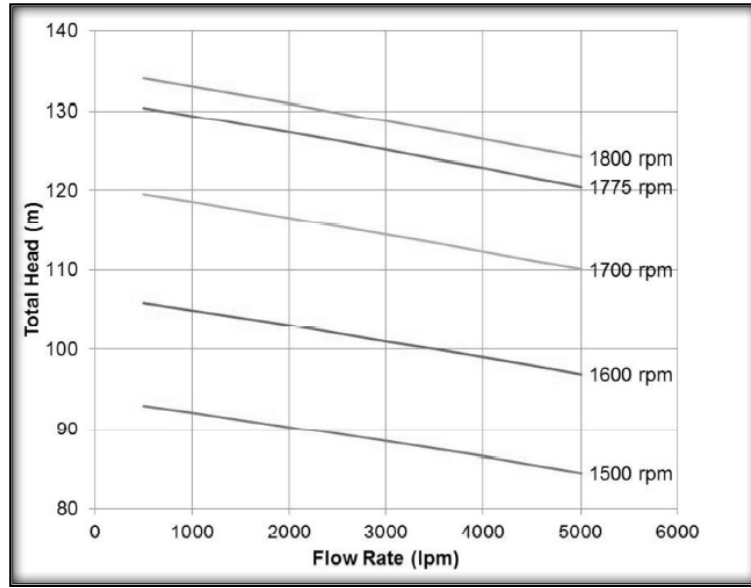


**Figure 13 - Subsea Pump Module Head Curves (Cohen. J, Stave. R, et al. May 2014)**

In Mjaavatten and Stammes, the following equation approximates the pump head for the above head curves shown in **Figure 13**. (Mjaavatten, Stammes et al. 2013)

$$f_{spm}(q_{spm}, \omega_{spm}) = c_0 \omega_{spm}^2 - c_1 \omega_{spm} q_{spm} - c_2 q_{spm}^2$$

where:

$$c_0 = 4.17 \times 10^{-5}$$

$$c_1 = 6.83 \times 10^{-2}$$

$$c_2 = 115$$

$\omega_{spm}$  is pump speed measured in RPM

$q_{spm}$  is flow rate measured in  $\frac{meters^3}{sec}$

$f_{spm}$  is pump pressure head measured in meters

## ***1.2.2 Field Testing and Operation***

The EC-Drill or CML system has had multiple implementation stages where in each deployment, the DGD technology and process has evolved. Major developmental stages are shown below in ascending order:

2003: Riserless Mud Recovery (RMR) deployment for BP in Caspian Sea

2004: RMR demo in Norwegian continental shelf (NCS)

2006 – 2008: RMR demo in deepwater

2009 – 2014: CML demo for Joint Industry Project (JIP)

2010: Managed pressure cementing deployment for BP in Caspian Sea

2011 – 2012: EC-Drill deployment on Scarabeo 9 semi-submersible

2012 – 2014: EC-Drill pilot testing in Troll field, Norway on Statoil JIP

(To date): EC-Drill deployment in Gulf of Mexico (GoM) and NCS

We will also specify the equipment and configuration specifics for critical components in the CML system (Rajabi.M, Stave. R, et al., June 2012):

### Subsea Pump Module (SPM)

1. Three-stage modified centrifugal pump (10.5 tons)
2. Each pump stage powered by 400 hp electric motor
3. Can handle gas cut mud up to 10%

### Modified Riser Joint (MRJ)

- SPM attached to MRJ and run in with riser
- MRJ was modified to allow a 6" diameter outlet
- Contains two remotely controlled hydraulic block valves

### Mud Return Line

- 6" ID with each joint measuring 164 ft.
- Run simultaneously with drilling riser with SPM attached

Shown in **Figure 14** (left) is the EC-Drill SPM along with running the riser with the SPM attached in the moonpool (right). In **Figure 15**, the EC-Drill SPM is shown in closer detail, again, attached to the marine drilling riser in the moonpool.



**Figure 14 - EC Drill SPM (Left) and Running Riser With SPM Attached (Right)**  
(Rajabi.M, Stave. R, et al., June 2012)

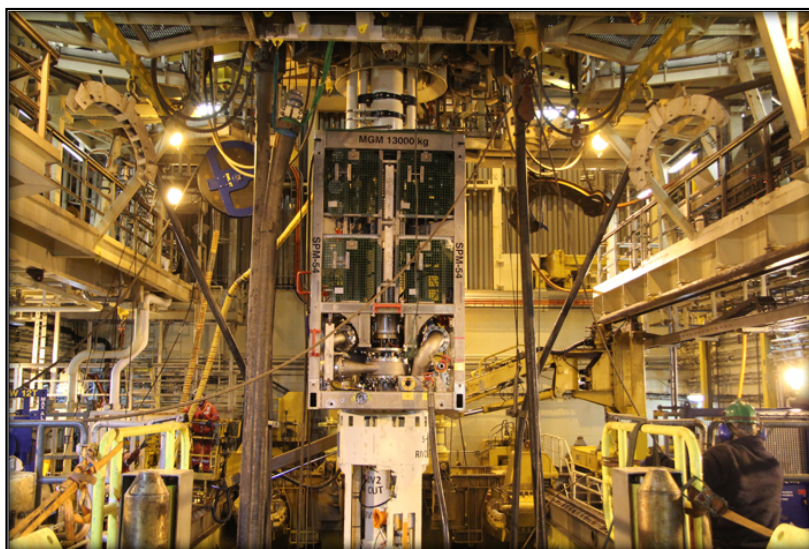


**Figure 15 - EC- Drill SPM in Moonpool Attached to Drilling Riser (Enhanced Drilling, 2014)**

### **1.3 Well Control Issues**

Unequivocally, maintaining well integrity under a set of controlled conditions is critical in achieving geological targets economically. Although there are numerous other causes of NPT that are subcategories of well control (ballooning and differentially stuck pipe), we will focus on what we consider are the two primary well control issues that need to be deliberated for DGD implementation – well kicks and lost circulation.

MPD has proven to be an effective process in meeting well objectives with minimal well control issues. DGD is no different in its efficacy, but first, we must understand the physics behind both well kicks and lost circulation before illustrating DGD's intrinsic value.

#### **1.3.1 Well Influxes**

A well influx or *kick* can be defined as the occurrence of pore pressure exceeding the hydrostatic acting upon the borehole. It is clearly understood that fluid flows from high pressure to low pressure, and therefore, the formation pressure drives formation fluid into the wellbore. There is often confusion between the semantics of *blowout* and *kick* and thus, we find it necessary to explain that a blowout is a kick that was not properly controlled and therefore, results in an uncontrolled well influx. There are three criteria needed in order to have a kick:

- Fluid must be mobile within the pore spaces of the formation rock
- Permeability must be high enough that mobile fluid can flow
- Aggregate pressures acting on the borehole wall must be less than the pore pressure of formation

If any of the above three criteria are not met, a kick is not physically possible. Secondly, we must discuss the criteria for the severity of a well kick. A rock with high permeability and high porosity is more likely to result in a more severe kick than a rock with low permeability and porosity. We see evidence of this when we examine sandstone and shale. Like any fluid, flow rate is dependent on the pressure differential between the formation fluid pressure and mud hydrostatic- the higher the difference in pressure between pore and mud weight, the higher the associated kick flow rate.

The following are common reasons for kicks:

1. Lower mud weight than needed
2. Poor hole filling practices when tripping
3. Swabbing during tripping operations
4. Loss of mud density due to gas cutting
5. Lost circulation

Real-time well monitoring and reliable tripping practices are of critical importance to kick detection. The subsequent cautionary signs are not unique to a single form of drilling technique and therefore, must unanimously be observed by all drilling personnel (Mitchell. R, Miska. S, et al. December 2010):

- Increase in pit volume
- Well flows despite rig pumps off
- Reduction in string weight
- Flow rate increase
- Pump-pressure decrease due to displacement of heavier mud

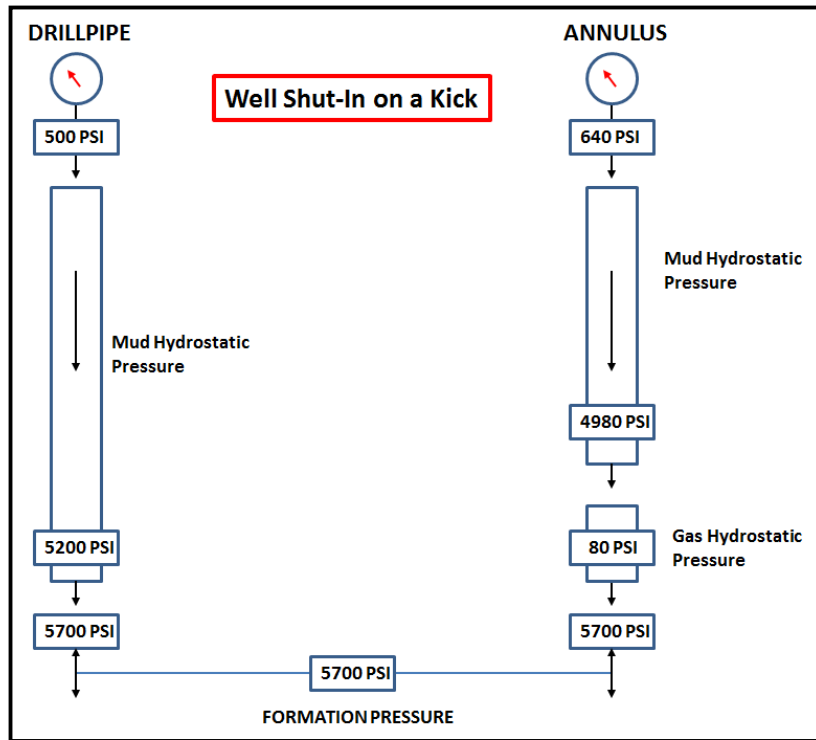


**Figure 16 - Graphical Display of a Well Kick Where Both Annulus and Drill Pipe Show Differential Needed to Balance Hydrostatic and Formation Pressure (Drilling Handbook)**

We show in **Figure 16** a graphical representation of a gas influx where the well is shut-in on detection of a kick where SIDP and SICP denote shut-in drill pipe and casing pressure.

### **1.3.2 Lost Circulation**

Lost circulation occurs when the mud density exceeds formation pressure. We see this relationship below in terms of pressure:

$$\rho_{Mud} > \rho_{fracture} > \rho_{wellbore-stability} > \rho_{pore}$$

If we examine the geo-mechanics of a wellbore, we observe that lost returns occur in the direction of maximum horizontal stress. We see the following relationship of the stress regime:

$$\sigma_{vertical} > \sigma_{H,max} > \sigma_{H,min}$$

An alternative view of the above expression is if the pressure within the borehole exceeds the pressure attempting to close it, the hole opens. The above expression holds true due to the stress anisotropy between the vertical overburden and the two horizontal stresses. If the mud weight is significant and abides by the first expression above, the circumferential stress or *hoop stress* is put into tension by the increasing internal pressure in the borehole. If the internal pressure increases beyond the tensile limit of the rock, fractures are induced and losses occur in the direction of  $\sigma_{H,max}$ . We observe this relationship in the figure below.

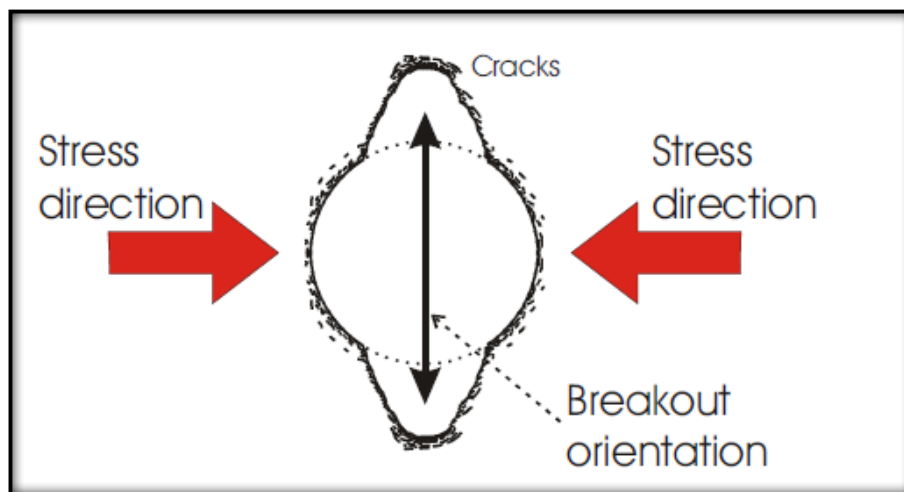


**Figure 17 - Breakout Occurs in the Direction of  $H_{min}$  While Lost Returns Occur in the Direction of  $H_{max}$  (British Geological Survey)**

Both well kicks and lost circulation result in considerable NPT to well operations, making it crucial to maintain well integrity throughout the drilling process. As previously discussed, deepwater environments trend towards narrow drilling windows and it is not uncommon to experience both influx and lost returns whilst drilling due to the nature of the pressure gradients. EC-Drill's ability to adjust internal pressure by controlling annular fluid height allows drilling in narrow pore/fracture pressure windows, reducing the likelihood of well influxes and lost circulation in real-time.

We will now discuss the methodology and results in our investigation of transient behavior using Schlumberger's *Drillbench Dynamic Drilling Simulation* software. This software highlights the importance of understanding the hydraulics during all drilling phases. As an industry, we neglect the dynamics nature of hydraulics due to its complexity and difficulty in modeling. However, as this thesis shows, modeling dynamic transient behavior with a high accuracy is crucial when drilling operations have increasingly diminishing operational margins in a low price environment.

## 2. METHODOLOGY

In this section, we will explain the methods we used alongside the technical basis and justification of our choices. We will address each chosen approach with what we consider to be the strength and weaknesses of each respective method. We illustrate the case for the given model in **Figure 18** below.

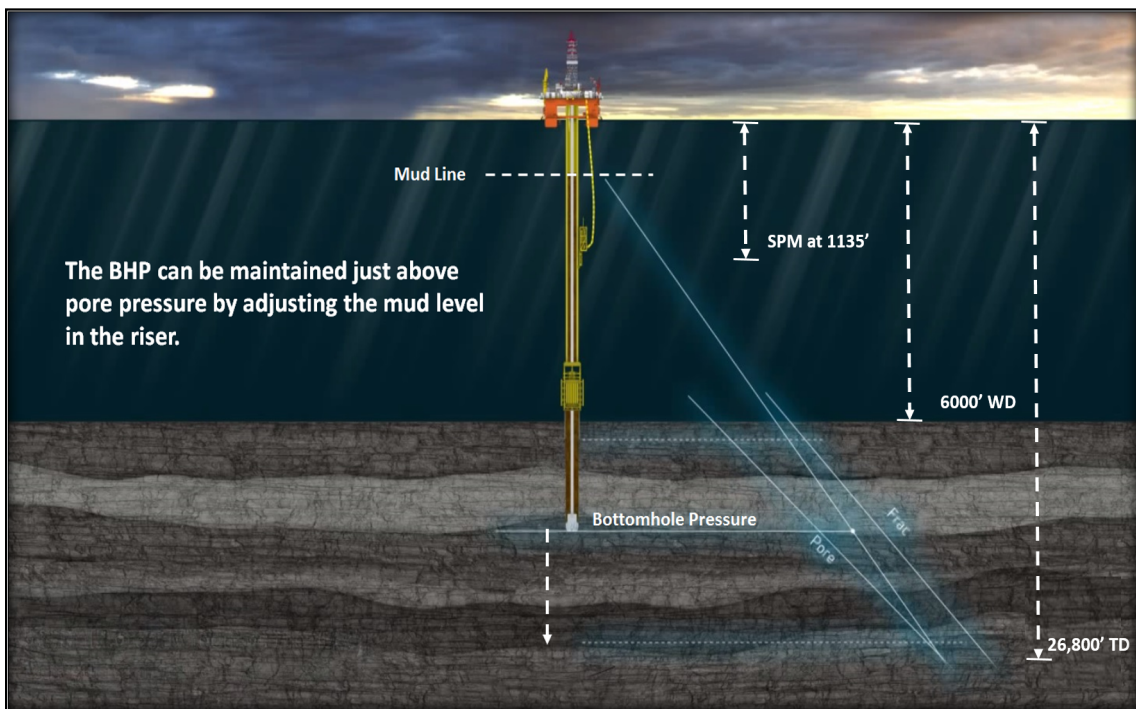


**Figure 18 - Graphical Display of Given Case where SPM at 1135', WD at 6000', TD at 26800' (Enhanced Drilling)**

There were three primary objectives for the investigation of transient behavior:

1. Illustrate how to simulate a connection with constant bottom hole pressure
2. Establish a given case within Drillbench™ and simulate connection
3. Optimize connection with respect to time and downhole pressure

## 2.1 Initial Planned Case Study

1. 6000' water depth, 19.5" ID riser
2. Drill with 12 ¼" bit and 14 ¾" hole opener
3. **Flow rate:** 750 gpm downhole
4. **Mud:** SOBM with MW 14.25 ppg, PV 22 cP, YP 17 lb/100ft<sup>2</sup>.
  - a. ESD full riser 14.45 ppg
  - b. With cuttings loading, max ECD is 14.90 ppg
5. Neglect/no cuttings
6. Subsea pump is mounted 1135' below RKB
  - a. 100 gpm top fill
  - b. 300 gpm boost
7. Do connection at 26800' with constant bottomhole pressure
8. Initial condition: circulating with 750 gpm, reduced riser level
9. Ramp down rig pumps from 750 gpm to 0 gpm gradually in 7.5 minutes – subsea pump reduces return flow to increase riser level at the same time
10. Wait for 5 minutes
11. Ramp up rig pump to 150 gpm in 3 minutes
12. Wait for 1 minute to fill drillpipe, break gel and establish increased return flow
13. Ramp up rig pump to 750 gpm in another 4 minutes
14. Plot flow in, flow out, riser level/pressure, downhole pressure, standpipe pressure – compare with field data. Discuss U-tubing in drill pipe, BHP accuracy and other effect

## 2.2 Revised Case Study

1. 4200' water depth, 19.5" ID riser
2. Drill with 12 ¼" bit and 14 ¾" hole opener
3. **Flow rate:** 750 gpm downhole
4. **Mud:** SOBM with MW 14.25 ppg, PV 22 cP, YP 17 lb/100ft<sup>2</sup>.
  - a. ESD full riser 14.45 ppg
  - b. With cuttings loading, max ECD is 14.90 ppg
5. Neglect/no cuttings
6. Subsea pump is mounted 1135' below RKB
  - ~~a. 100 gpm top fill~~
  - ~~b. 300 gpm boost~~
7. Do connection at 26800' with constant bottomhole pressure
8. Initial condition: circulating with 750 gpm, reduced riser level
9. Ramp down rig pumps from 750 gpm to 0 gpm gradually in 7.5 minutes – subsea pump reduces return flow to increase riser level at the same time
10. Wait for 5 minutes
11. Ramp up rig pump to 150 gpm in 3 minutes
12. Wait for 1 minute to fill drill pipe, break gel and establish increased return flow
13. Ramp up rig pump to 750 gpm in another 4 minutes
14. Plot flow in, flow out, riser level/pressure, downhole pressure, standpipe pressure – compare with field data. Discuss U-tubing in drill pipe, BHP accuracy and other effects

We disregard both the top fill and boost lines for two principal reasons. First, neither of the two additional flow inputs are available to be adjusted in Drillbench – a limitation of the software itself. Secondly, the addition of these two additional lines adds complexity outside the scope of this thesis. Neglecting the two additional

hydraulic inputs does not detract from the fundamentals of the transient behavior and therefore, we concluded to continue simulation.

## **2.3 Software**

As DGD is commercially limited, software for modeling dynamic behavior is limited to pre-existing software with an add-on module for dual-gradient drilling. There are numerous in-house proprietary models within the industry, however there are only a handful of software that is commercially available with the robustness and accuracy needed.

### ***2.3.1 Possible Options***

1. *K&M Technology Group* – designed for Chevron’s SMD projects
2. *Schlumberger Drillbench*® – contains a DGD module with dynamic behavior modeling
3. *User-built MATLAB and/or C++ models* - limited in flexibility and ease of use

In choosing suitable software, we had the following four criteria:

1. Able to model transient behavior
2. Flexible to a number of given cases
3. Ease of use and learning curve
4. Accessibility to educational institutions

Schlumberger’s Drillbench® met all four requirements, granted with the necessary in-house training. A clear advantage of the software is its ease of use interface, coupled with support for dual-gradient drilling with a subsea pump. Additionally, the software’s potential to read pore and fracture pressure from Techlog® was appealing for future work prospects.

As Schlumberger states,

*“Simulations performed in Drillbench dynamic drilling simulation software are key feature to replicate a real drilling operation and provide accuracy not possible with simpler steady-state models”*

Drillbench<sup>®</sup> offers the following applications (Schlumberger Software):

1. Accurate modeling of transient behavior
2. Sensitivity studies
3. Gel breaking effects
4. Surge and swab calculations
5. Temperature variations
6. Tool limitations
7. ECD management
8. Dual-gradient drilling
9. Pressure build-up

We will detail limitations of the software later, but for now, we think it important to note that the software meets both our given criteria and provides a robust solution for dynamic drilling simulation within a reasonable computational time. We provide the following software version and specifications below.

### ***2.3.2 Software Version***

The software version used was version number 6.2.1.127495 (Educational License). It consisted of the following features:

- Blowout control
- Dynamic hydraulics
- Dynamic well control
- Steady-state hydraulics
- Underbalanced drilling

### 3. SIMULATION DESIGN

We will show the following steps as guidance for the simulation design of the above cases. There are three primary input categories that are critical to having the simulation compile:

1. Basic Input
2. Expert Input
3. Run Configuration

We will showcase each input category and the corresponding sub-categories for input. The details of each section are paraphrased from the Drillbench Dynamic Hydraulics contents which can be accessed from *Help* → *Help Topics*

#### 3.1 Basic Input

Within this category, the following inputs need to be completed:

1. Summary – well description, temperature, mud weight, drill string, etc.
2. Description – well number and name, location, author, notes
3. Survey – well trajectory surveys (MD, Inclination, Azimuth)
4. Formation – surface temperature, lithology, geothermal gradient
5. Pore pressure and fracture pressure – gradients at specific depths
6. Wellbore geometry – casing and liner hanging depths, riser specifications
7. String – BHA, drill string configuration, and bit configuration
8. Mud – rheology, base density, oil/water ratio, PV, YP, Fann-reading, etc.
9. Temperature – mud injection temperature, depth reference, etc.

### 3.1.1 Summary

The summary input auto-completes a description of the field and well, the well geometry, the drilling fluid, drillstring, and geology as shown in **Figure 19**.

Description			
<b>Company</b>	Statoil		
<b>Field</b>	NCS		
<b>Well</b>	N/A	<b>Well section</b>	N/A

Well geometry		Drilling fluid	
<b>Riser length</b>	4200.00 ft	<b>Fluid</b>	SOBM Example - 14.45ppg
<b>Casing shoe</b>	21000.00 ft	<b>Type</b>	Oil based
<b>Initial bit depth</b>	26800.03 ft	<b>Oil/water ratio</b>	81.00/19.00
<b>Total MD</b>	26800.03 ft	<b>Density</b>	14.45 lbm/USgal
<b>Bit diameter</b>	12.250 in	<b>Casing ID</b>	14.000 in
		<b>Vertical depth</b>	26800.03 ft

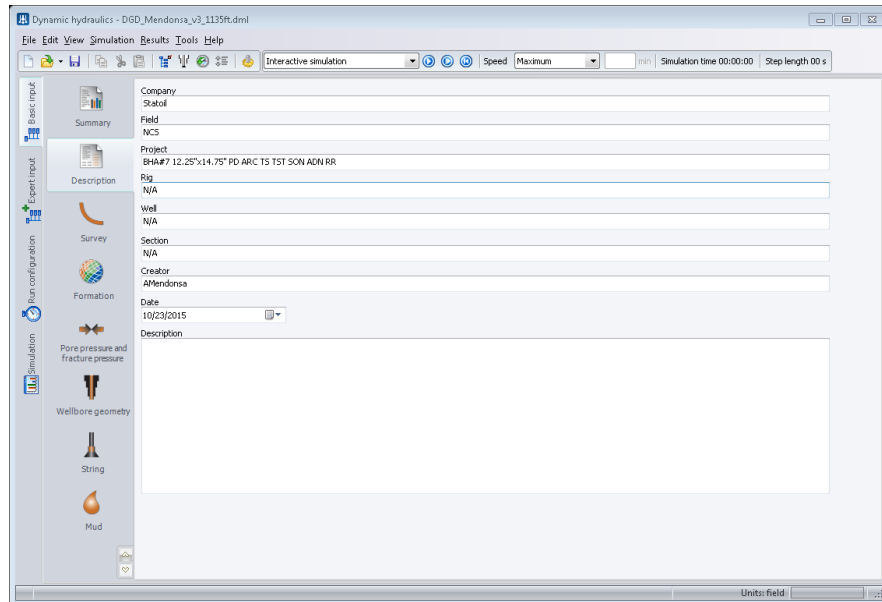
  

Drillstring		Geology	
<b>Number of drillpipes</b>	5	<b>Formation temperature</b>	<b>Casing shoe</b> 195.69 Fahrenheit
<b>Drillpipe 1 OD</b>	6.625 in		<b>TD</b> 259.49 Fahrenheit
<b>Drillpipe 2 OD</b>	6.625 in	<b>Fracture pressure</b>	<b>Casing shoe</b> n/a psi
<b>BHA max OD</b>	12.250 in	<b>Pore pressure</b>	<b>TD</b> n/a psi
		<b>Bit</b>	Bit 12 1/4
		<b>Length</b>	91.52 ft
		<b>Length</b>	337.67 ft
		<b>Length</b>	0.00 ft

**Figure 19 – Auto-Completed Summary Input**

### 3.1.2 Description

The description input is a simple way of detailing authorship, the operating company, field, well, and well section. Include any comments that are notable as shown in **Figure 20**.



**Figure 20 - Description Input**

### ***3.1.3 Survey***

In this section, input the planned survey intervals in the format of measured depth (MD), azimuth measured in degrees, and inclination measured in degrees from vertical. Drillbench calculates the TVD from the input through the industry standard of minimum curvature algorithm. Survey data can be imported through LAS format or entered manually as shown in **Figure 21**.

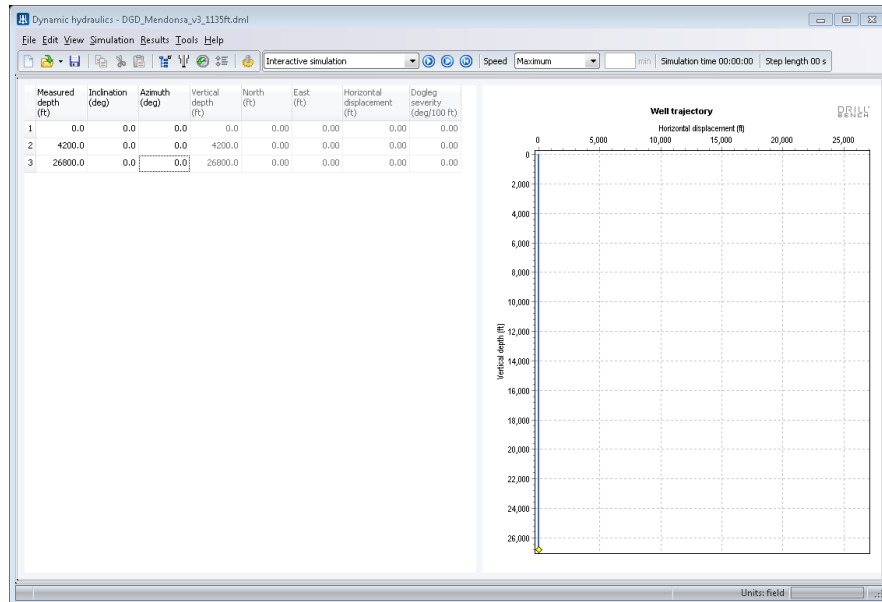


**Figure 21 - Survey Input With MD, Inclination and Azimuth**

### **3.1.4 Formation**

In this section, input the surface temperature measured in °F as well as the top and bottom intervals (TVD) of each formation. For example, in the case of DGD, we input an air gap, seawater, and the actual formation. This specific section is necessary if a dynamic temperature model is used. In terms of surface temperature, offshore wells should be measured at sea water temperature as shown in **Figure 22**.

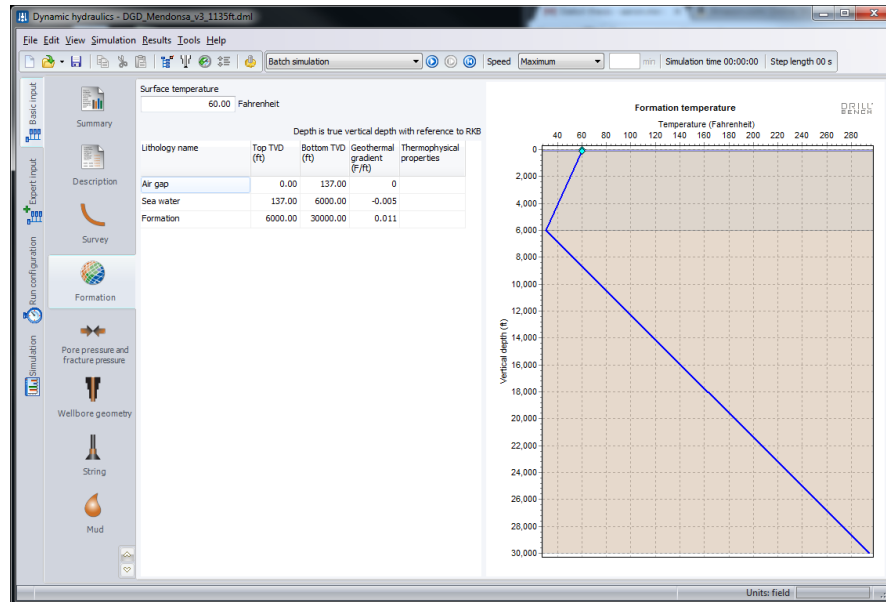


**Figure 22 - Geology and Thermophysical Properties**

### ***3.1.5 Pore Pressure and Fracture Pressure***

In this section we input the appropriate drilling window at specific depths in units of either psi or ppg. From this information, the software performs a model fit to the inputs and extrapolates that model to each discrete depth for the entire well as shown in **Figure 23**.

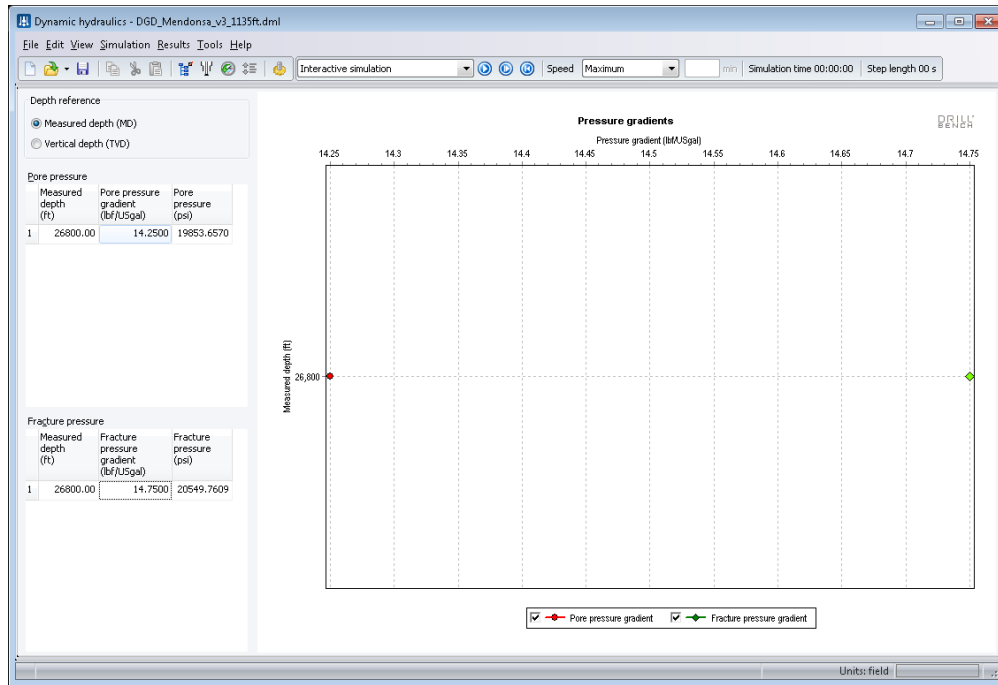


**Figure 23 - Pore Pressure and Fracture Pressure Window**

### **3.1.6 Wellbore Geometry**

In this section we input the riser details such as length, ID, OD, and thermophysical properties. Additionally, we input the hanger and setting depth along with OD and ID of each casing/liner string. We also note the top of cement, the material above the cement, and thermophysical properties as shown in **Figure 24** and **Figure 25**.

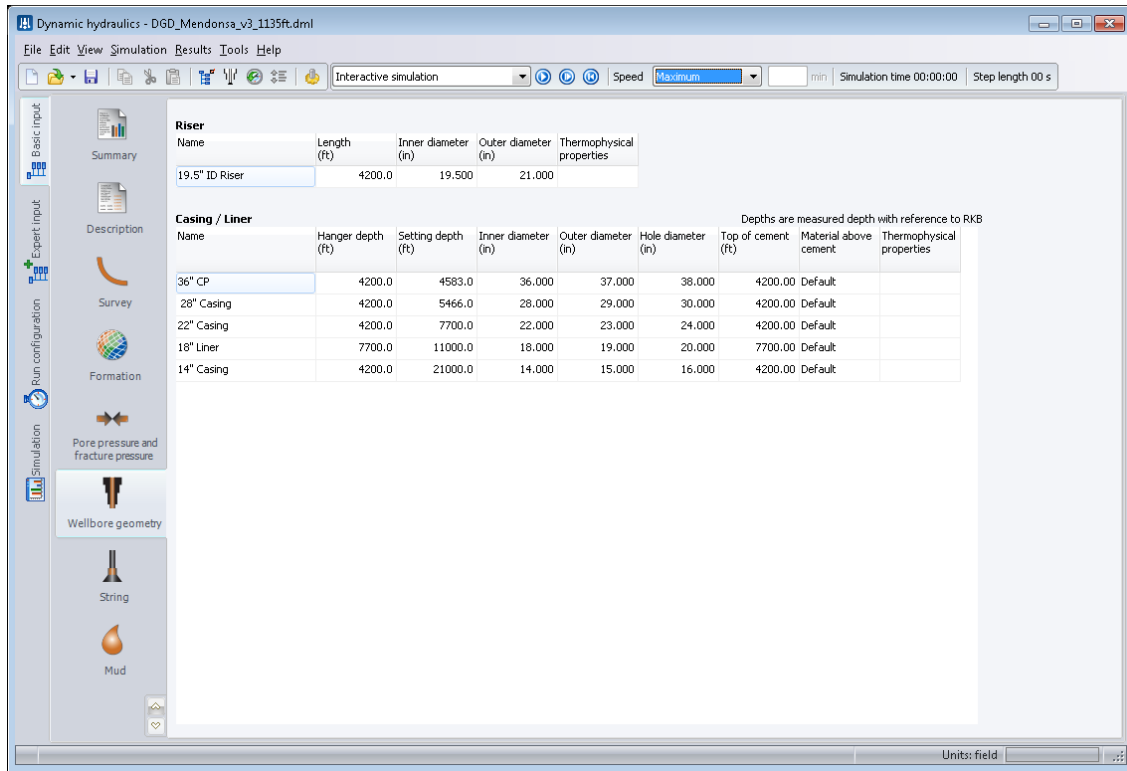
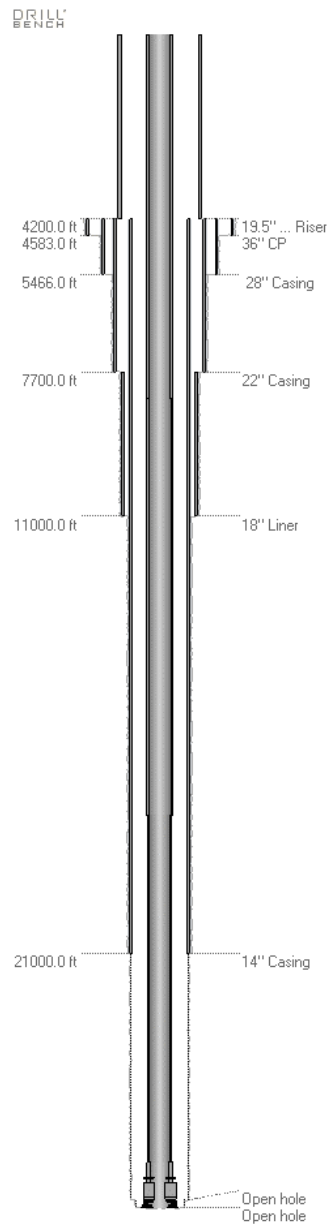


Figure 24 - Wellbore Geometry



**Figure 25 - Wellbore Schematic With Casing Strings**

### 3.1.7 Drillstring

In this section we input each component of the BHA along with type, section length, ID and OD. There are five primary components for the string design:

1. Bit
2. Jetsub
3. Motor
4. MWD
5. Underreamer

Additionally, we input the nozzle diameters, the bit diameter, and verify the total flow area of the chosen bit as shown in **Figure 26**.

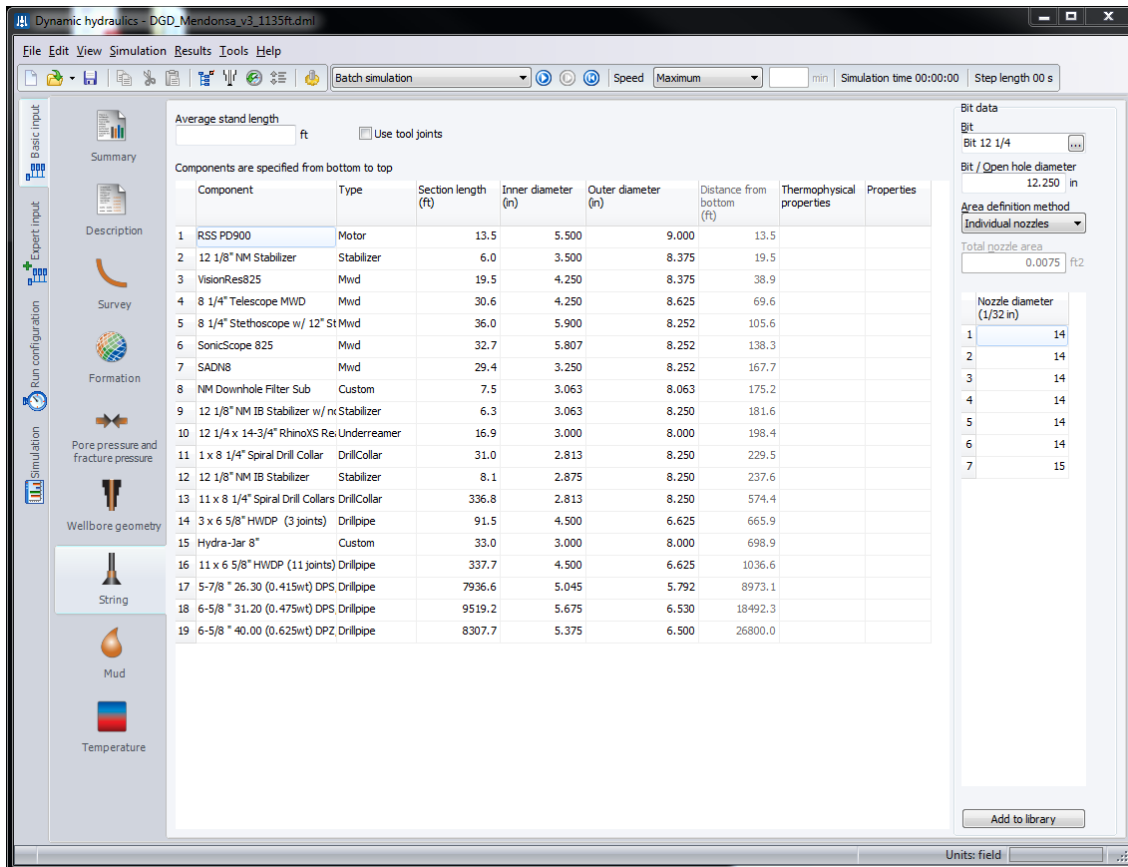


**Figure 26 - Drillstring, BHA, and Bit Configuration**

Attached is the BHA configuration with a total string length of 26,800' with a 12.25" bit and 14.75" underreamer in **Figure 27**. Complete specifications can be found in the appendix.

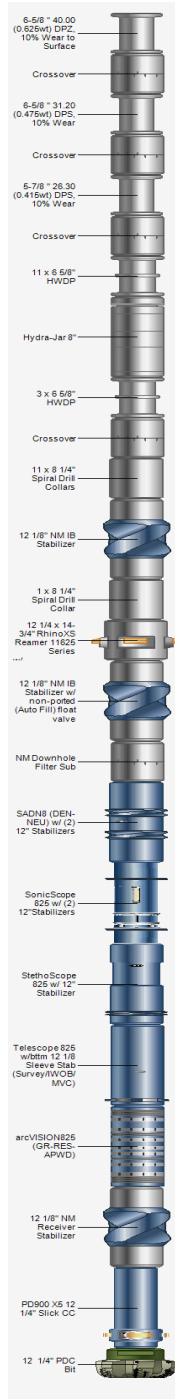


**Figure 27 - BHA Configuration (Statoil and Schlumberger)**

### 3.1.8 Drilling Fluid

In this section, we will input the fluid properties of the mud. These include:

1. Base density (14.7 psia and 60 °F).
2. Solids density (defaults at 4.2 sg – barite)
3. Overall density
4. Reference temperature
5. Oil/water ratio
6. PVT model data
7. Rheology model
8. PV, YP, Fann reading

There are three rheology models that can be used to calculate mud rheology with respect to pressure and temperature as shown in **Figure 28**.

1. Power law
2. Bingham
3. Robertson-Stiff (recommended) – uses three Fann readings

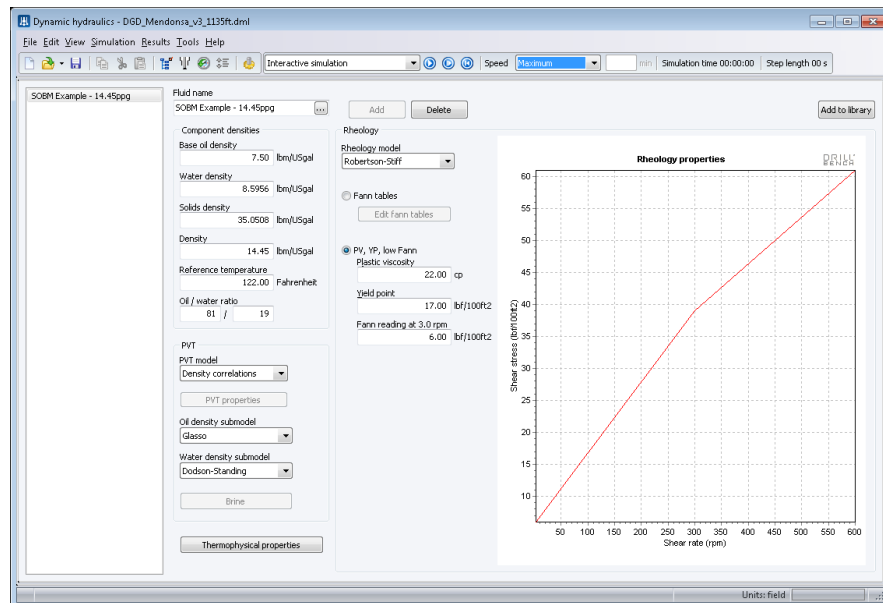


Figure 28 – Mud Properties

### 3.1.9 Temperature

In this section, we have three primary inputs that output a dynamic model for the wellbore as shown in **Figure 29**.

- Constant mud injection temperature – measured in Fahrenheit
- Constant temperature difference – between mud injection temperature and mud outlet temperature
- Surface temperature model
  - Heat loss constant
  - Initial pit temperature

From those mentioned, Drillbench creates a dynamic model initialized from geothermal gradient. The software divides the total well into grid cells that are two dimensional comprising of radial and flowline. Each grid cell is dynamically calculated with a specific heat transfer and temperature.

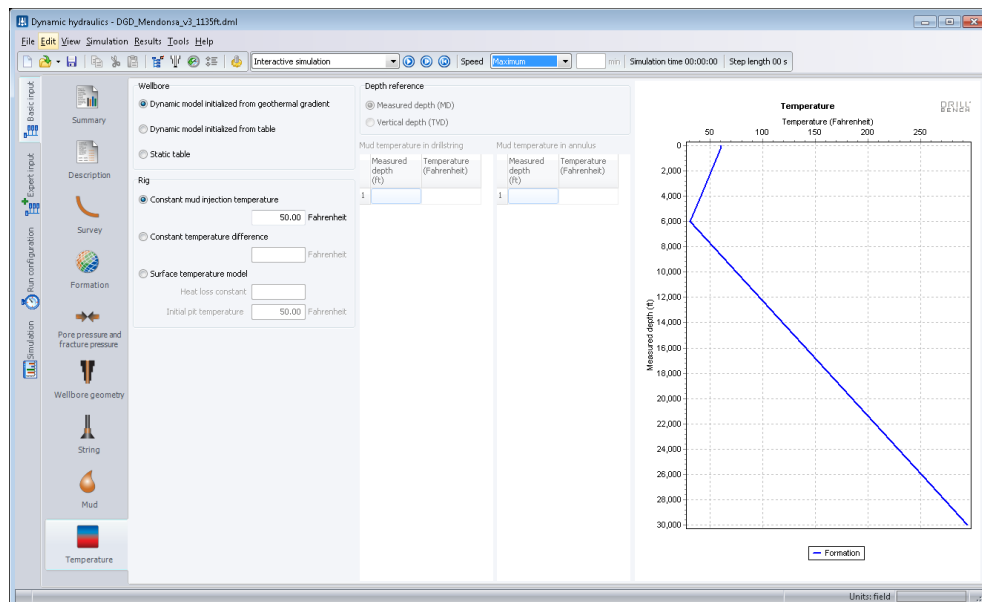


**Figure 29 - Temperature Model**

## 3.2 Expert Input

There are five primary categories of inputs that are considered optional for the simulation. In this specific case however, we will solely utilize the DGD gradient with sub-sea pump.

1. Model Parameters – number of grid cells in flow direction
2. Eccentricity – deviated section or table calculations of eccentricity factor %
3. Surface pipeline – rate and pressure loss
4. RCH and choke – choke and control parameters
5. Dual gradient with subsea pump
  - Mud/air
  - Initial top of blanket fluid and density
  - Initial top of mud
  - Subsea pump mode
    - Pump rate change
    - Pump position

### 3.2.1 Model Parameters

This section is often overlooked but is quite important for the backend mathematical model. By defining the number of grid cells used, the user is defining the level of discretization of the well. Increasing the grid cell number will increase the accuracy of the simulation, but will also increase computational time. Drillbench, in best-case scenario have a linear relationship to grid cell count. Schlumberger recommends 90 grid cells out of the possible 2000. Note that this simulation was run with 200 grid cells

### ***3.2.2 Eccentricity***

If we assume, like in our simulation, that the drill string is concentric with the annulus, this section is optional. If we wanted to account for eccentricity, the software would use the maximum eccentricity above a given deviation.

### ***3.2.3 Surface Pipeline***

We neglected the pressure loss between the surface piping and the pump. However, if one wanted to account for the pressure loss, the software would linearly interpolate between the two nodes.

### ***3.2.4 RCH and Choke***

We neglected this section since we did not use a rotating control head (RCH). If, however, the case requires it, one can define the pressure change with respect to choke opening. Additionally, this module has an automatic control parameter set where the following inputs are required:

1. Constant bottomhole ECD
2. Proportional gain
3. Integral gain
4. Derivative gain

### ***3.2.5 Dual Gradient Mode with Subsea Pump***

There are four primary categories of input for DGD simulation:

1. Dual gradient mode
2. Fluids
3. Riser backpressure
4. Sub-sea pump

We detail the categories above in further detail of choices below:

#### Dual Gradient Mode

1. Mud/air
2. Mud/blanket fluid
3. Mud/blanket fluid/air

#### Fluids

- Initial top of blanket fluid
- Blanket fluid density
- Initial top of mud

#### Riser Backpressure

- Input associated backpressure – in this case, atmospheric pressure 14.70 psi

#### Subsea Pump

1. Pump mode
  - Automatic – stabilize the boundary pressure at the subsea pump depth
  - Manual - change the pump rate manually
2. Pump rate change (GPM)
3. Pump position (ft) – measured from RKB

The following assumptions are made for the pressure calculation in the DGD riser:

- Fluids from the well into the DGD riser are normalized to standard conditions with respect to density (neglecting temperature)
- Fluids are stacked according to density upon entrance of the riser with heavy density at the bottom in the discretization process
- The software supports an automatic refill of blanket fluid from a top refill pump (optional)

Note: The software also inputs a “flow stop device” that opens according to whether the rig pumps are circulating or off. For our model and for the way the software computes pressure, the device is always open. (Schlumberger, 2015)

### **3.3 Run Configuration**

There are three configuration modes that can be used within the software:

- Batch configuration
- Dynamic surge and swab
- Cementing job

We primarily used batch configuration as our simulation focuses on the transient behavior at a connection. Therefore, we neglected dynamic surge and swab and cementing.

#### ***3.3.1 Batch Configuration***

In this mode, the user must define a set of conditions with respect to time. For example, the software logically follows operational conditions from each time cell. Meaning, the input for the current computation relies on the output of the prior cell. In this study, we define the first set of conditions as follows:

- **Grid Cells:** 200
- **Time step length:** 0.1 mins or 0.06 seconds
- **Speed:** time constrained to the time step length above

The batch configuration requires the following for simulation output:

1. Duration (mins)
2. Rig pump rate (GPM)
3. Fluid density (ppg)
4. Inlet temperature (°F)
5. Rotation velocity (RPM)
6. Torque (ft-lbs)
7. Rate of penetration (ft/hr)
8. Boundary pressure at subsea pump depth (psi)

Shown in **Table 1** below is a summary of the run configuration of the final simulation batch configuration that follows the set of conditions defined above in terms of grid cell and time step. The full run configuration can be found in the Appendix.

**Table 1 - Batch Configuration Run**

Duration (mins)	Flow Rate (GPM)	Fluid Density (ppg)	Inlet Temp(degF)	RPM	Torque	ROP	Boundary Pressure at Subsea pump depth (psi)	Bit Depth (ft)
10	750.00	14.45	60	145	0	0	740.13	26800.03
0.5	696.43	14.45	60	145	0	0	747.98	26800.03
0.5	642.86	14.45	60	145	0	0	755.82	26800.03
0.5	589.29	14.45	60	145	0	0	763.67	26800.03
0.5	535.71	14.45	60	145	0	0	771.52	26800.03
0.5	482.14	14.45	60	145	0	0	779.37	26800.03
0.5	428.57	14.45	60	145	0	0	787.22	26800.03
0.5	375.00	14.45	60	145	0	0	795.06	26800.03
0.5	321.43	14.45	60	145	0	0	802.91	26800.03
0.5	267.86	14.45	60	145	0	0	810.76	26800.03
0.5	214.29	14.45	60	145	0	0	818.61	26800.03
0.5	160.71	14.45	60	145	0	0	826.46	26800.03
0.5	107.14	14.45	60	145	0	0	834.30	26800.03
0.5	53.57	14.45	60	145	0	0	842.15	26800.03
1	0.10	14.45	60	145	0	0	850.00	26800.03
1	0.10	14.45	60	145	0	0	851.00	26800.03
1	0.10	14.45	60	145	0	0	851.00	26800.03
1	0.10	14.45	60	145	0	0	851.00	26800.03
1	0.10	14.45	60	145	0	0	851.00	26800.03
0.5	25.02	14.45	60	145	0	0	848.14	26800.03
0.5	49.93	14.45	60	145	0	0	844.40	26800.03
0.5	74.85	14.45	60	145	0	0	840.66	26800.03
0.5	99.77	14.45	60	145	0	0	836.92	26800.03
0.5	124.68	14.45	60	145	0	0	833.17	26800.03
1	149.60	14.45	60	145	0	0	829.43	26800.03
0.5	150.00	14.45	60	145	0	0	829.37	26800.03
0.5	150.00	14.45	60	145	0	0	829.37	26800.03
0.5	225.00	14.45	60	145	0	0	818.11	26800.03
0.5	300.00	14.45	60	145	0	0	806.84	26800.03
0.5	375.00	14.45	60	145	0	0	795.58	26800.03
0.5	450.00	14.45	60	145	0	0	784.31	26800.03
0.5	525.00	14.45	60	145	0	0	773.05	26800.03
0.5	600.00	14.45	60	145	0	0	761.78	26800.03
0.5	675.00	14.45	60	145	0	0	750.52	26800.03
10	750.00	14.45	60	145	0	0	739.25	26800.03

## 4. RESULTS AND DISCUSSION

The objective of this section is to investigate transient behavior for the given case. We will present the results in a clear and concise manner that has relevance based upon the simulation design discussed in the prior section. In the last subsection, we will discuss and critically evaluate literature studies and attempt to show that the results shown below answer the research objective. To reiterate, the results shown below are based upon the output of the simulation design mentioned above.

### 4.1 Mud Level

In **Figure 30** below, we show the annular mud height for the riser as well as the U-tubing effect of the drillstring during stages of a connection. The stages are described below.

1. Initial condition – 750 GPM
2. Ramp down rig pumps from 750 GPM to 0 GPM in 7.5 mins
3. Wait 5 minutes – make connection
4. Ramp up rig pumps to 150 GPM in 3 mins
5. Wait 1 minute to break gel strength
6. Ramp up pumps from 150 GPM to 750 GPM in 4 minutes
7. Final condition – 750 GPM

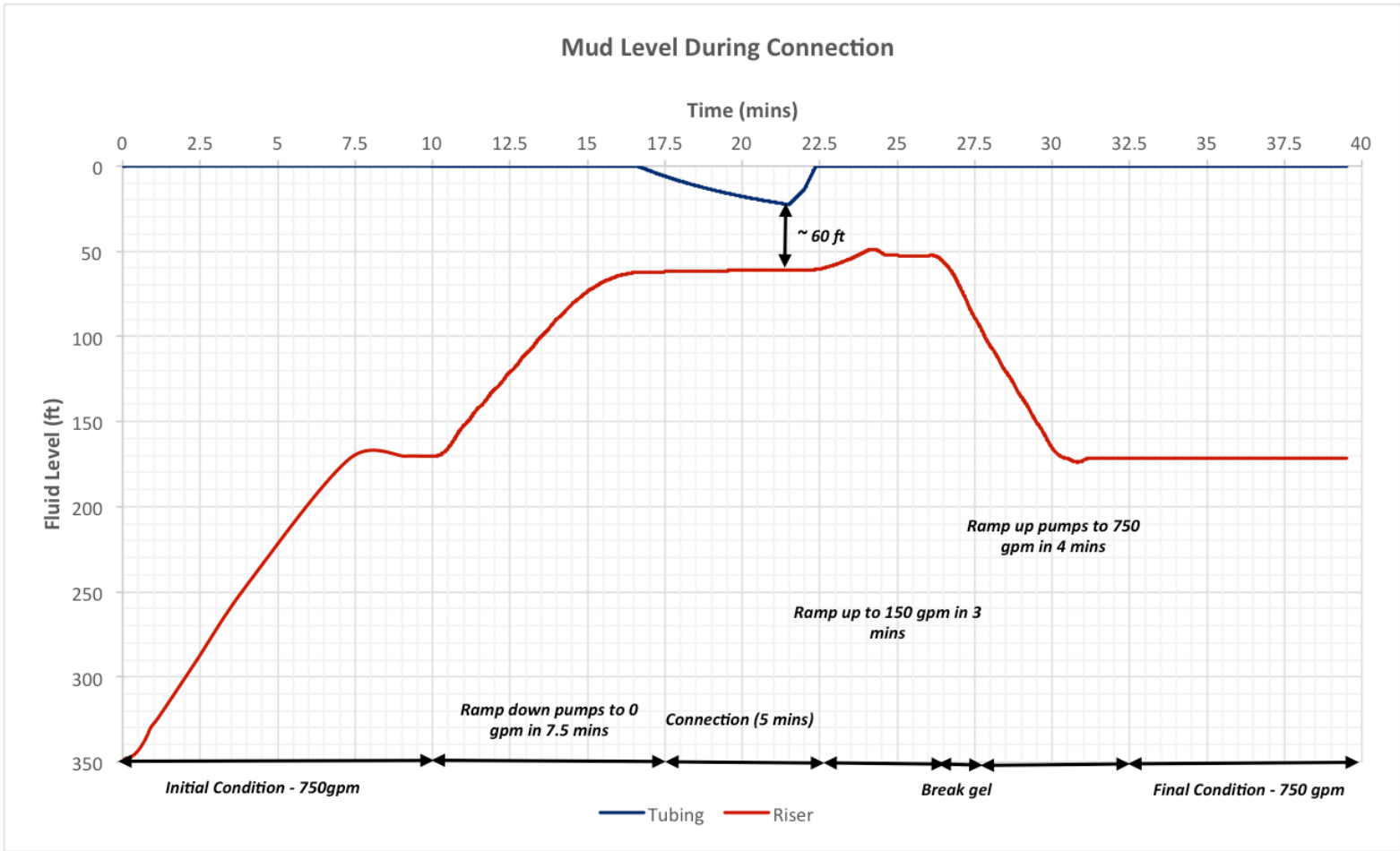
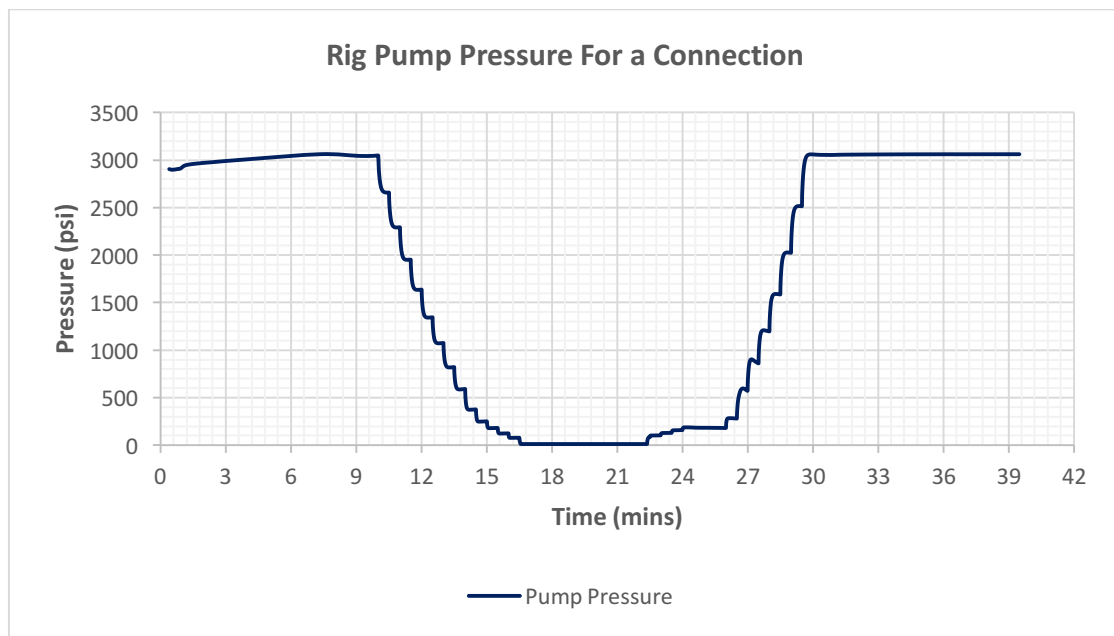


Figure 30 - Mud Level During Connection for Drillstring and Riser

Due to the U-tube effect – the annular mud height, and therefore pressure, is lower than the drillstring, there is an equilibrium effect to balance the hydrostatic head in both. Results show the total drop in mud height in the drillstring was approximately 60 feet. **Figure 30** corresponds to both the rig pump pressure shown next and the subsea pumps shown later.

## 4.2 Rig Pump Pressure



**Figure 31 - Ramping of Rig Pumps During a Connection**

**Figure 31** describes the rig pump pressure measured in PSI. The above figure corresponds to the stages described above in section 4.1. As we discussed in the literature review, the flow rate is dependent on the rig pump pressure. We illustrate the rig pump rate in section 4.3.

### 4.3 Rig Pump Rate

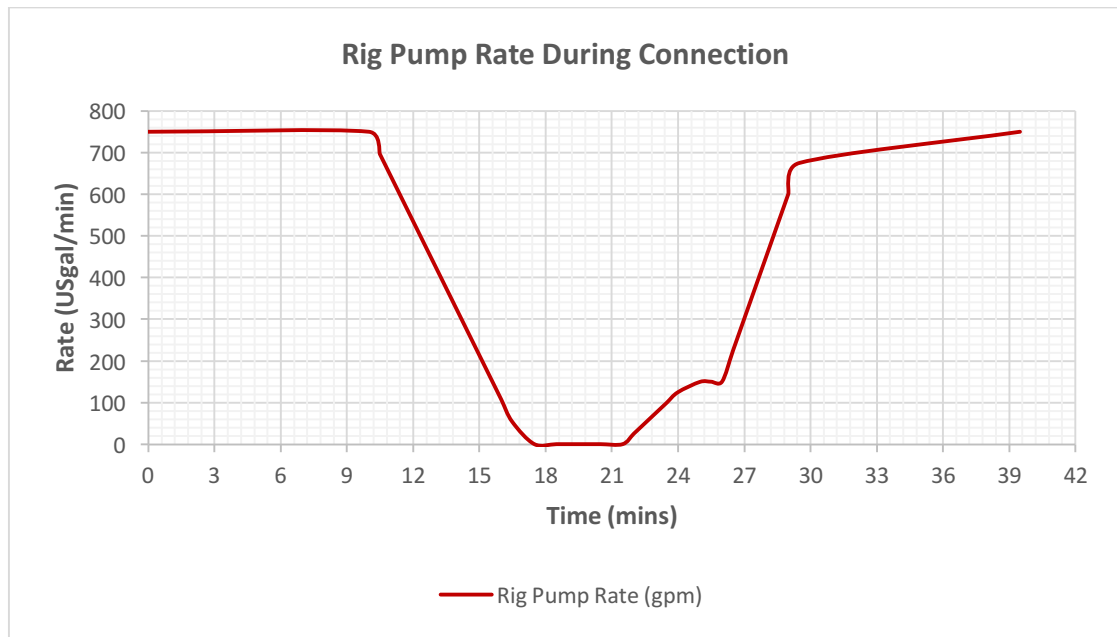


**Figure 32 - Rig Pump Rate During Connection**

**Figure 32** details the ramping up and down of the rig pumps during a connection. As mentioned above, we establish the base initial condition at 750 GPM for 10 minutes. The pump rate remains at 0 GPM for 5 minutes and the shape changes from the initial trend due to an operational requirement of breaking the gel strength of the mud for 1 minute.

#### 4.4 Subsea Pump Module Pressure

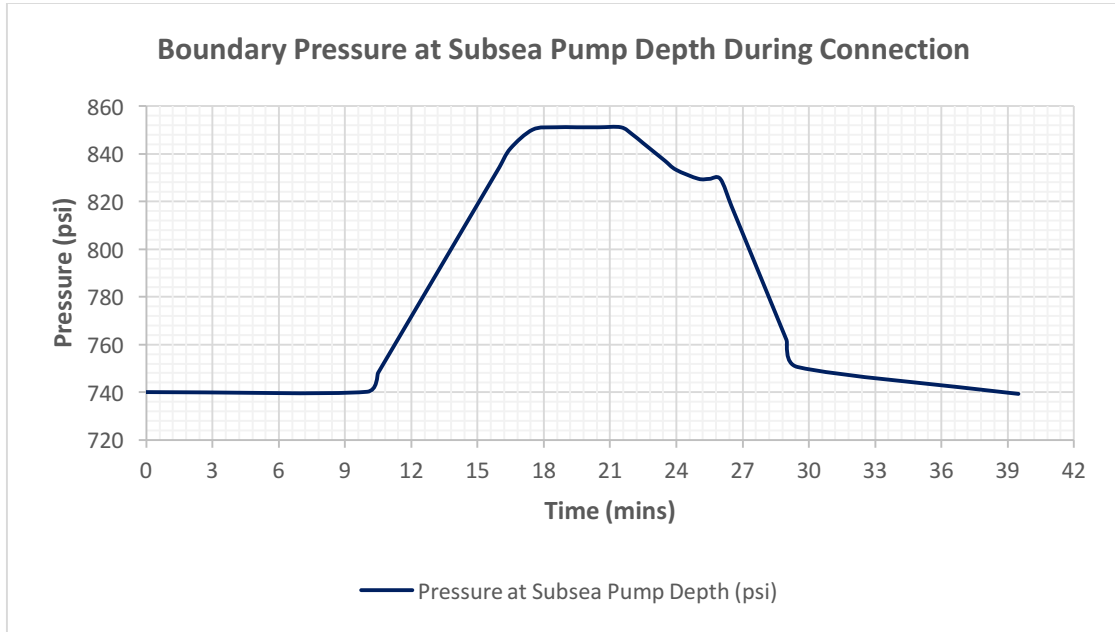


**Figure 33 - Boundary Pressure at 1135' During Connection**

In **Figure 33** above, we show the subsea pressure at 1135' with respect to time. We assume that the mud level is stable during the initial phase of 750 GPM. As the rig pump starts ramping down, the suction pressure or *boundary pressure* increases for the SPM to counter-act the loss of rig pump pressure. Equally, the flow rate of the subsea pump rate or discharge rate decreases to maintain a chosen annular mud height. We note the static level between 18-21 minutes. As the rig pump pressure starts to increase after the connection, the subsea pump module correspondingly decreases the boundary pressure now to account for the additional pressure provided by the rig

pumps. We observe this negative trend from 22.5 minutes until the 27.5 minutes where steady-state dominates.

#### 4.5 Subsea Pump Module Rate

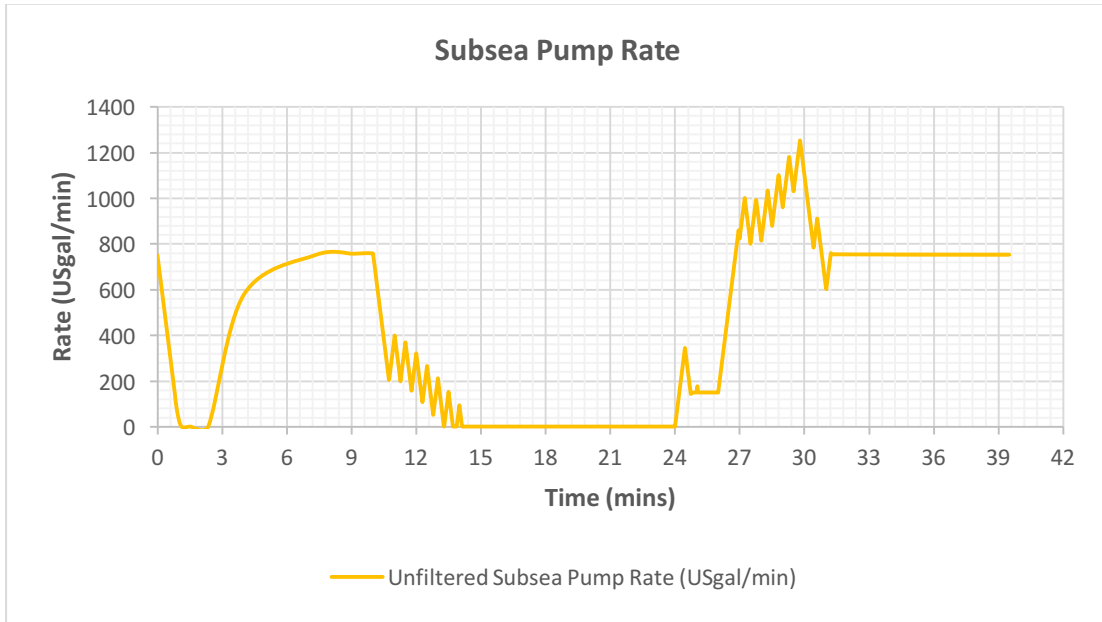


**Figure 34 - Unfiltered Subsea Pump Rate**

In **Figure 34** above, we present the subsea pump rate measured in GPM. Unlike the boundary pressure and rig flow rate that was user-inputted, the subsea pump rate was calculated throughout the simulation. Therefore, we are not surprised to see the noisy display and ‘spiky’ nature.

Filtering the noise was simple as the output values simply did not make sense within the constraints of the simulation run. Thus, we filtered the outliers in each time step and removed them accordingly. **Figure 35** shows the filtered subsea pump rate.

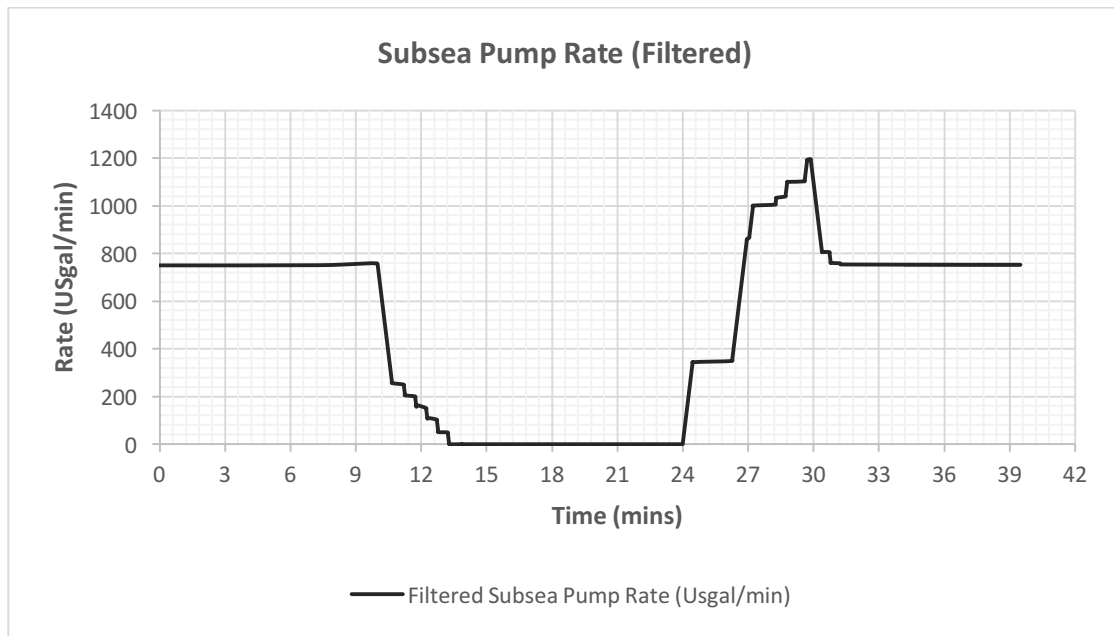


**Figure 35 - Filtered Subsea Pump Rate**

We observe in **Figure 35** that the initial flow rate is in steady-state – this makes physical sense as the mud level does not change for the first ten minutes. As the rig pump slows down, the mud level starts to drop accordingly. To counter-act this reduction in annular mud height, the subsea pump must also slow down to maintain a static mud level. We see this ramp down between 10 – 24 minutes.

Once the drilling connection is made, the rig pumps ramp up for circulation. As the flow rate increases, the mud level will also start to increase as well. Again, to counter-act this, the subsea pump must ramp up to maintain the desired static mud height. We note that maintaining a static annular mud height is equivalent to maintaining a constant bottomhole pressure. As the transient behavior terminates, the subsea pump and rig pump transition back to steady-state.

## 4.6 Bottomhole ECD

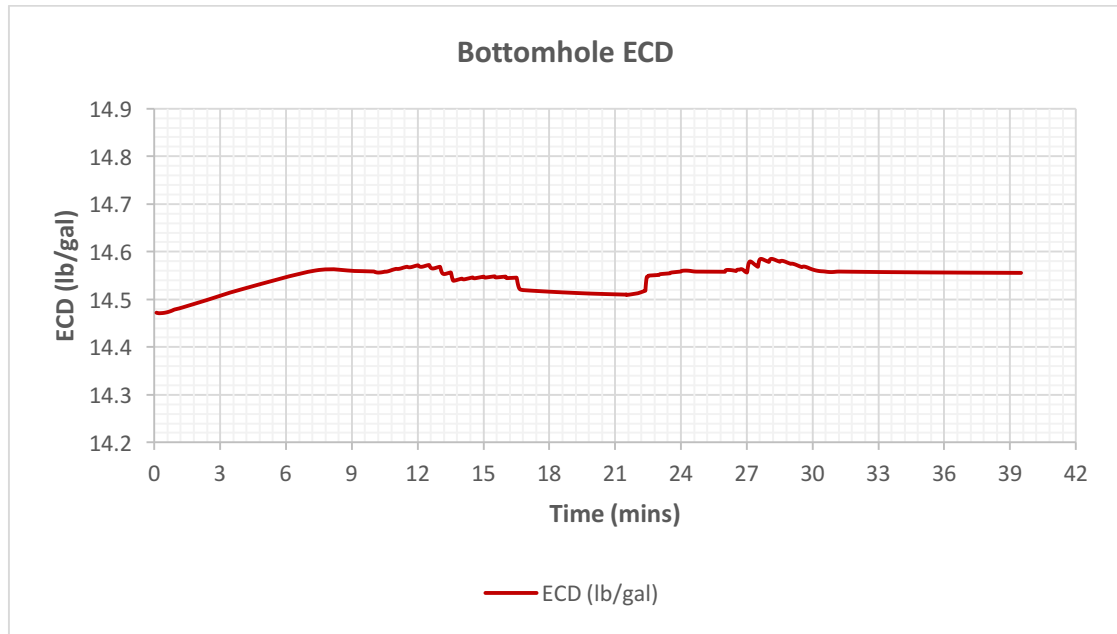


**Figure 36 - Bottomhole Equivalent Circulating Density During Connection**

We observe that **Figure 36**, that despite transient and dynamic changes in both pumps, the bottomhole equivalent circulating density remains fairly unchanged. This simulation output meets the given criteria where the ECD during connection does not exceed 14.90 ppg with cuttings loading. **Figure 36** shows promise to address well control issues where either the ECD drops below pore pressure gradient or above fracture pressure gradient, measured in ppg.

## 4.7 ECD Profile

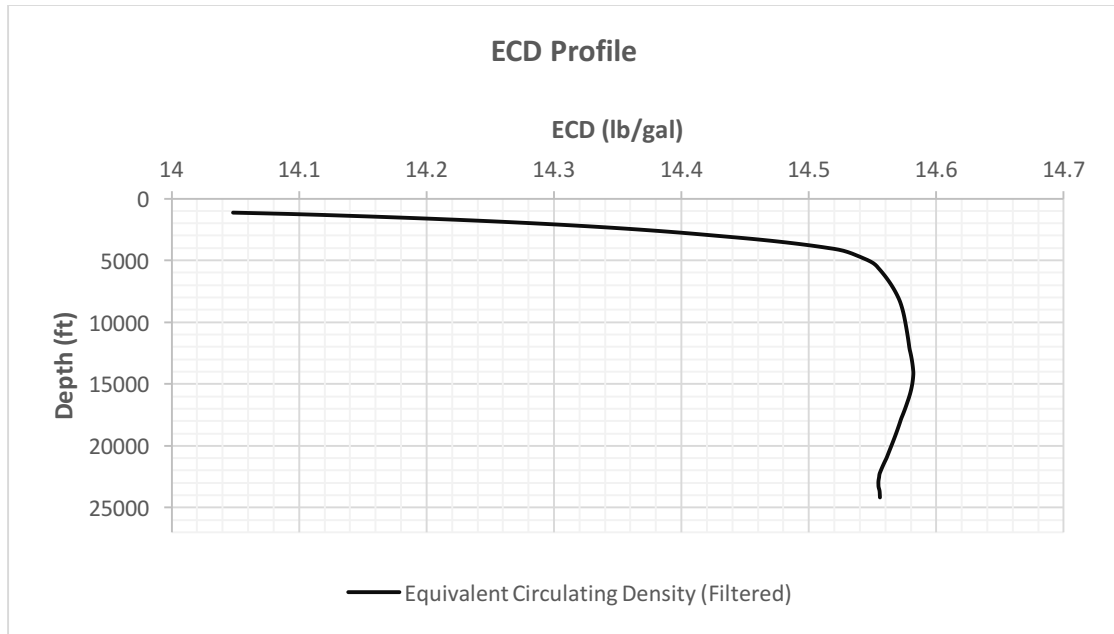


**Figure 37 - Equivalent Circulating Density Profile by Depth**

In **Figure 37**, we illustrate the equivalent circulating density in ppg by depth. We note that the starting point is at the total water depth of 4200'. As we progress to 26,800' or total depth, we verify that the ECD with a partially-evacuated riser is between 14.45- 14.6 ppg. This makes physical sense as the hydrostatic head of the full mud column at 26,800' would predictably be between 14.45 – 14.6 ppg as well.

## 4.8 Bottomhole Pressure

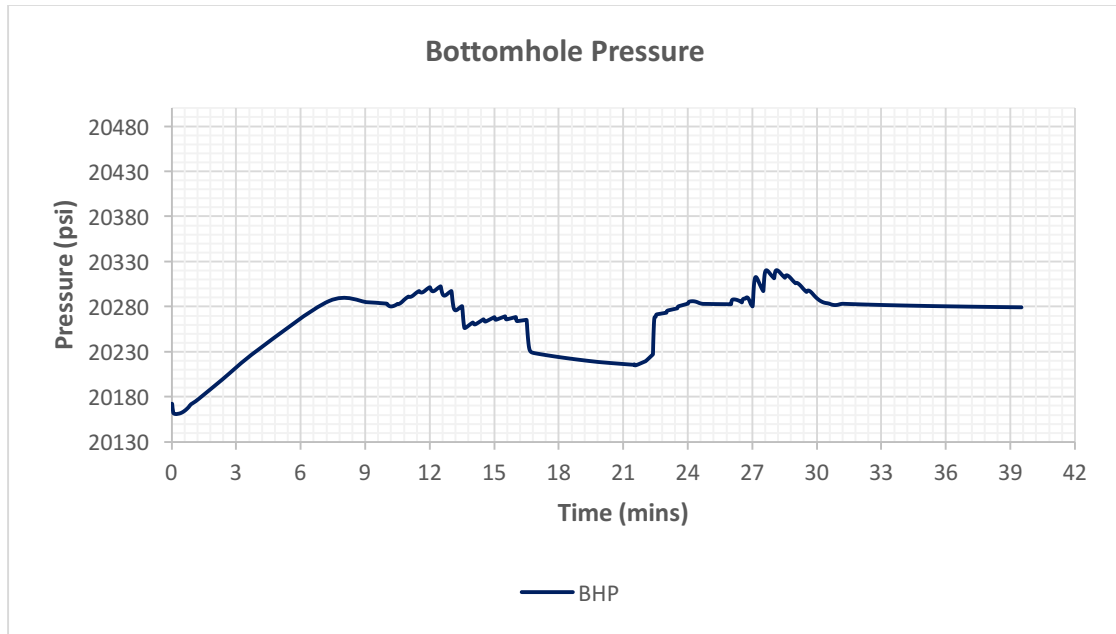


**Figure 38 – Bottomhole Pressure During Connection**

We observe from **Figure 38** that BHP does fluctuate throughout transient operations. However, we can effectively ignore the linear increasing trend from 0 – 10 minutes as the simulation requires some initial condition to compile. If we observe the BHP from 10 minutes onwards, we note that the largest deviation is 60-70 psi. Although this seems high, we note the depth at 26,800' where that magnitude of deviation is negligible. Recalling Figure 36, we can verify that bottomhole ECD remains largely unchanged throughout connection.

## 4.9 Well Pressure Profile

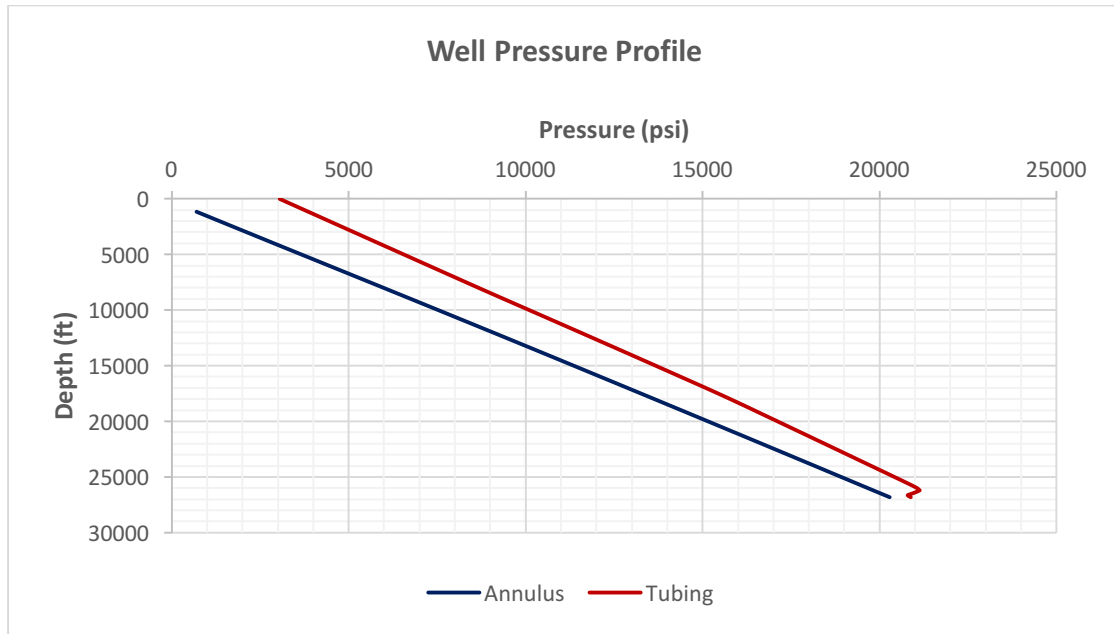


**Figure 39 - Well Pressure Profile by Depth**

We observe the pressure profile for both the drillstring and annulus in **Figure 39**. The well pressure profile accounts for the pressure drop through each interval of the well. We note that the difference between annulus and drillstring is largely due to the partial-evacuation of the riser at the total water depth of 4200'. The separation or disconnect between annulus and drillstring at TD is due to the software neglecting the bit pressure loss.

## 4.10 Mud Flowrate

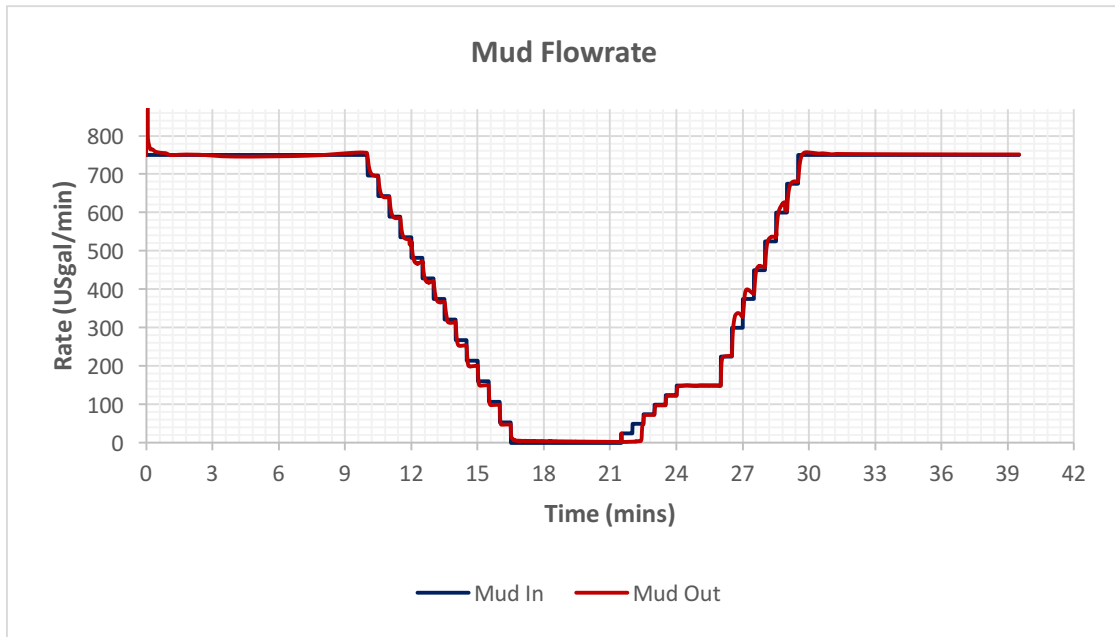


**Figure 40 - Mud Flowrate In and Out**

In **Figure 40**, we illustrate the mud flowrate in GPM both in and out. It is noteworthy to mention that both the input and the output overlay each other except during the interval of 21 – 23 minutes. From prior figures, we note that during this interval the subsea pump rate delays ramp up until approximately 24 minutes. After this interval, both the input and output of mud are relatively equivalent.

## 4.11 Bottomhole Temperature

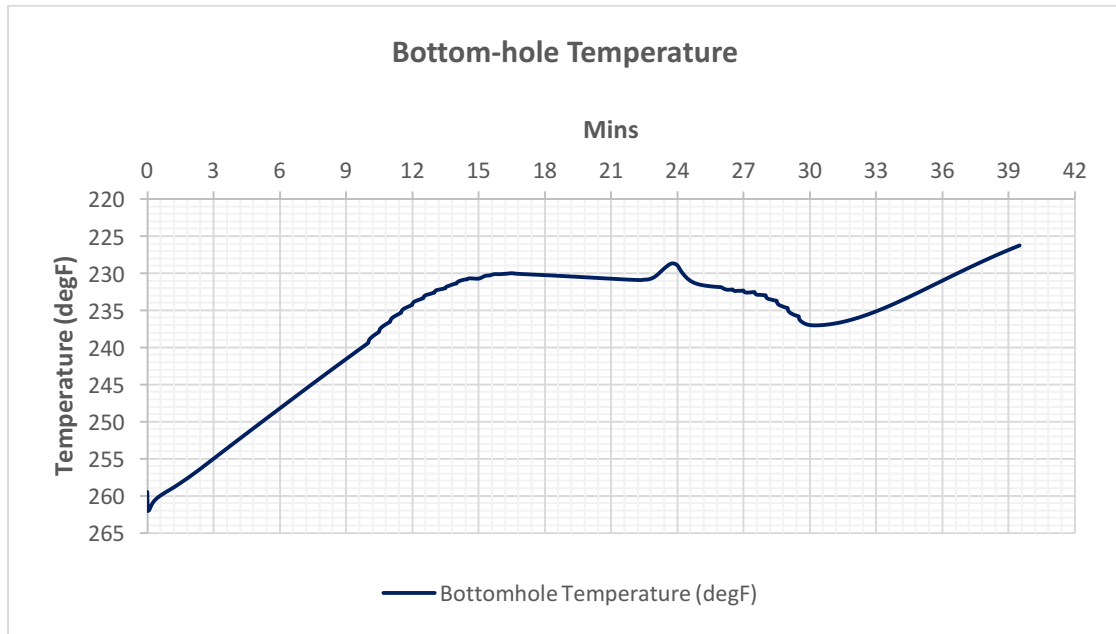


**Figure 41 – Bottomhole Temperature at 26,800' During Connection**

We show in **Figure 41**, the bottomhole temperature measured in Fahrenheit at 26,800' depth throughout each stage. The initial positive slope is due to the simulation requiring an initial condition in order to compile. There is not much variation between temperature but we do note that the decrease in temperature from 27 minutes. Most likely, this positive slope decrease is due to new mud that has passed through the water column arriving at the bottomhole.

## 4.12 Temperature Profile

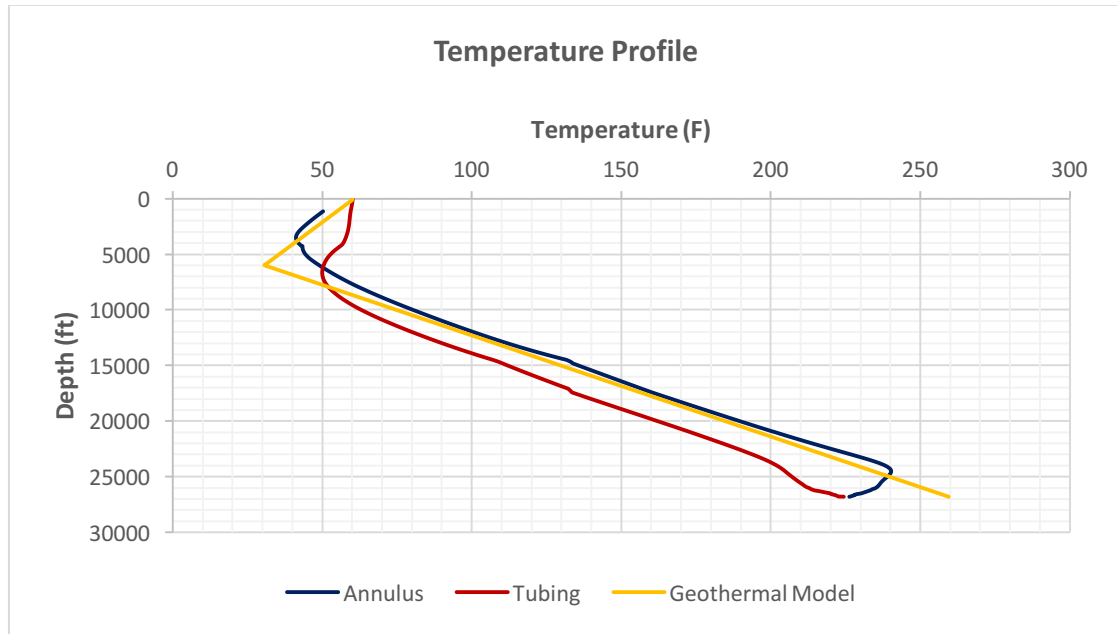


**Figure 42 - Temperature Profile by Depth**

We illustrate the temperature profile of the annulus, drillstring, and the dynamic geothermal model by depth in **Figure 42**. The initial difference between the annulus and drillstring is most likely due to heat transfer differences as the drillstring is centralized within the annulus. In order for the drillstring to receive heat transfer, the temperature from the seawater must conduct both through the riser, the mud, and then the drillstring. The geothermal model is calculated dynamically based upon the input conditions and discrete grid size.

### 4.13 Pit Gain

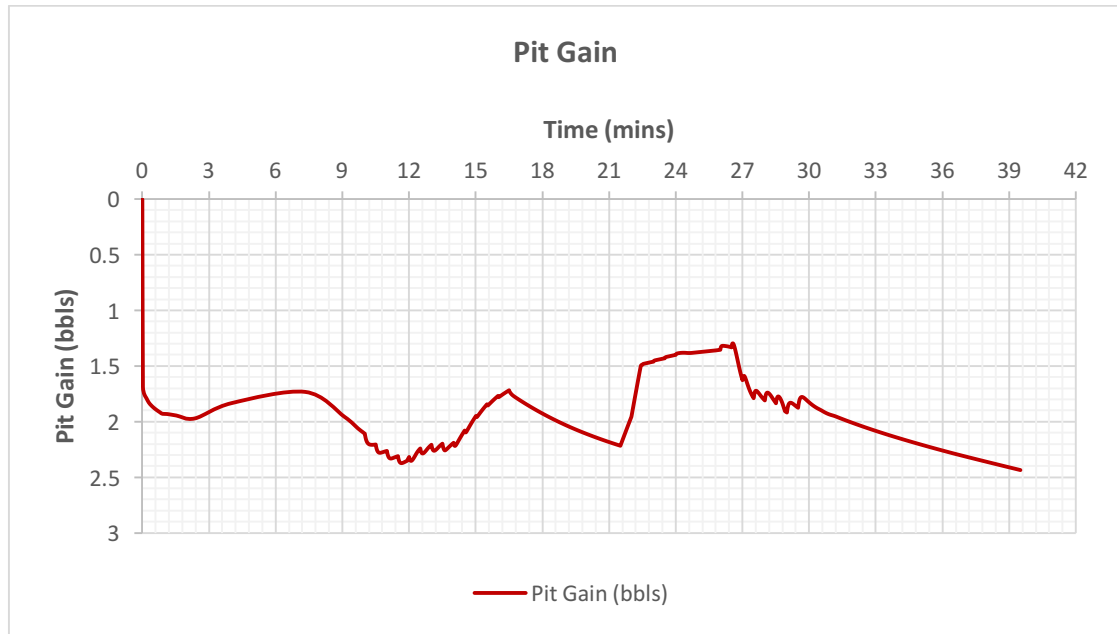


**Figure 43 - Pit Gain Measured in Barrels**

In **Figure 43**, we simulate the pit gain measured in barrels throughout each stage. The single notable observation point would be the stages between the rig pump ramping down and up, and the subsea pump correspondingly responding. During connection or between 18-21 minutes, we notice an increase in pit level, most likely due to the rig pump not pumping any intake while the subsea pump is discharging mud. However, the deviation between the pit gain levels is insignificant at 0.5 bbls at most.

#### 4.14 Pressure Drop across Bit

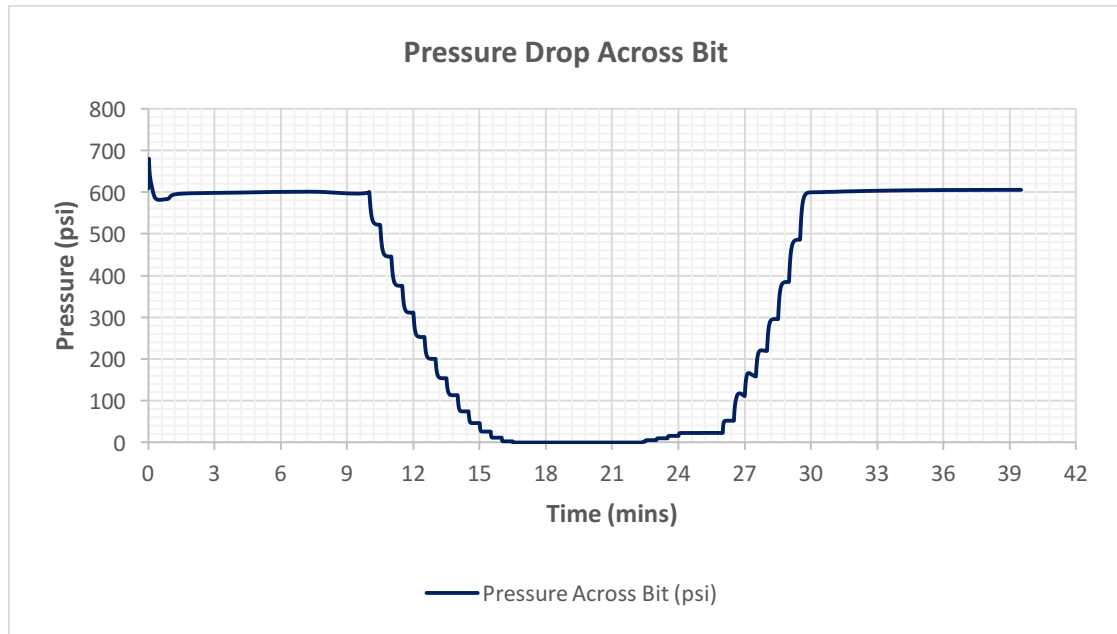


**Figure 44 - Pressure Loss across Bit in Psi**

We observe in **Figure 44**, that the initial pressure loss at 750 GPM is approximately 600 psi. As the rig pump starts to ramp down in preparation for the connection, the pressure loss of the bit correspondingly decreases due to the parallel drop in flow velocity. In contrast, as the rig pump starts to ramp up in preparation to drill ahead, the pressure loss increases due to the additional friction resulting from an increase in flow velocity through the nozzles.

## 4.15 Pumped Volume

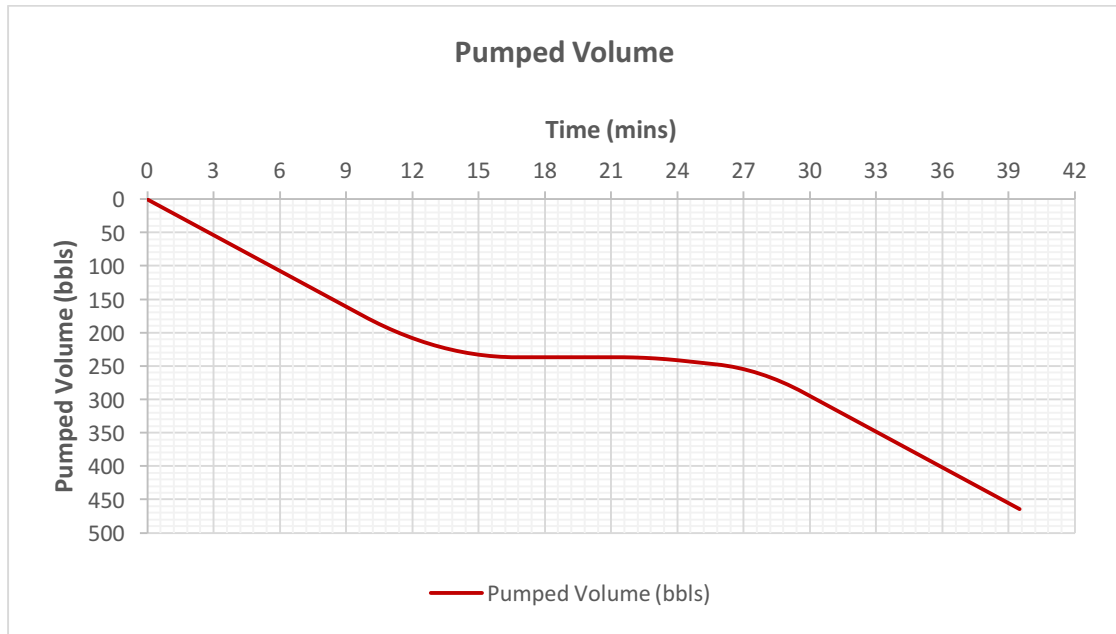


**Figure 45 - Pumped Volume Measured in Bbls**

We observe the predictable trend in **Figure 45** of an increasing pumped volume measured in barrels throughout the operation. We note the unchanged volume from between 18 – 21 minutes where the rig pumps are off due to a drilling connection being made. As the connection is made, the rig pumps ramp up in preparation of drilling ahead. Analogously, the pumped volume increases in response to the rig pumps circulating.

#### 4.16 Equivalent Viscosity

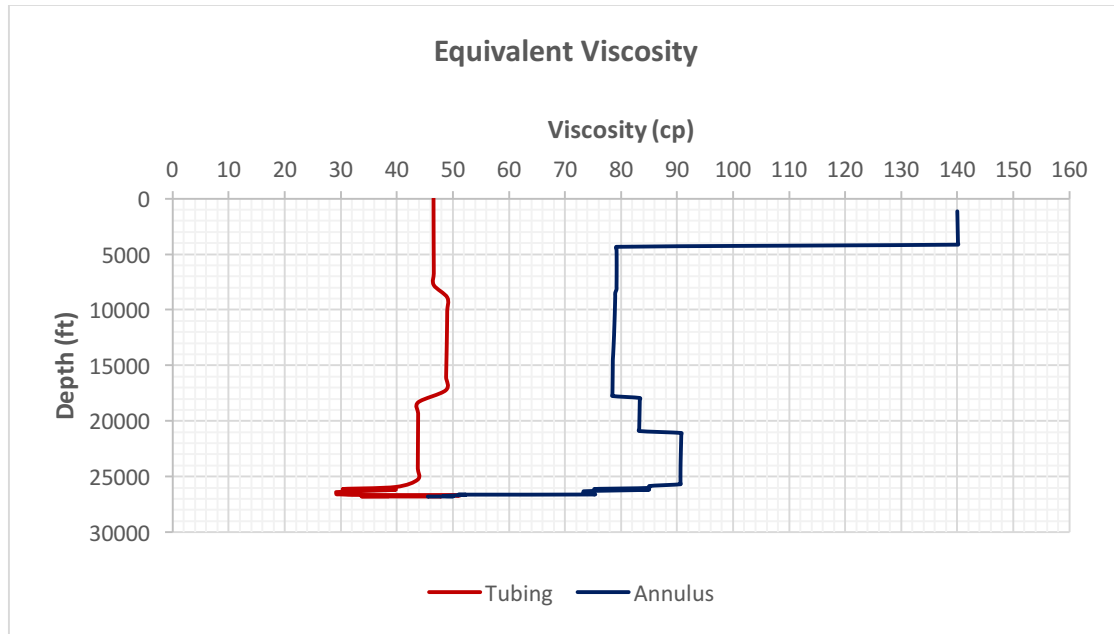


**Figure 46 - Equivalent Viscosity Profile by Depth**

We observe the equivalent density by depth in **Figure 46**. Recall that viscosity is largely dependent on temperature. Depending on whether the fluid is considered Newtonian or non-Newtonian, pressure can also have a significant effect upon the viscosity. We note that the viscosity in the drillstring is lower than the viscosity in the annulus, despite being the same fluid due to temperature difference. For the seawater temperature to transfer to the mud, conduction and convection must occur through the riser, the mud, and the drillstring. In contrast, for the geothermal temperature to transfer to the mud, conduction and convection must occur through casing, mud, and

the drillstring. This series of heat resistances results in the deviation in viscosity, measured in centipoise between the drillstring and annulus by depth.

#### 4.17 Reynolds Number Profile

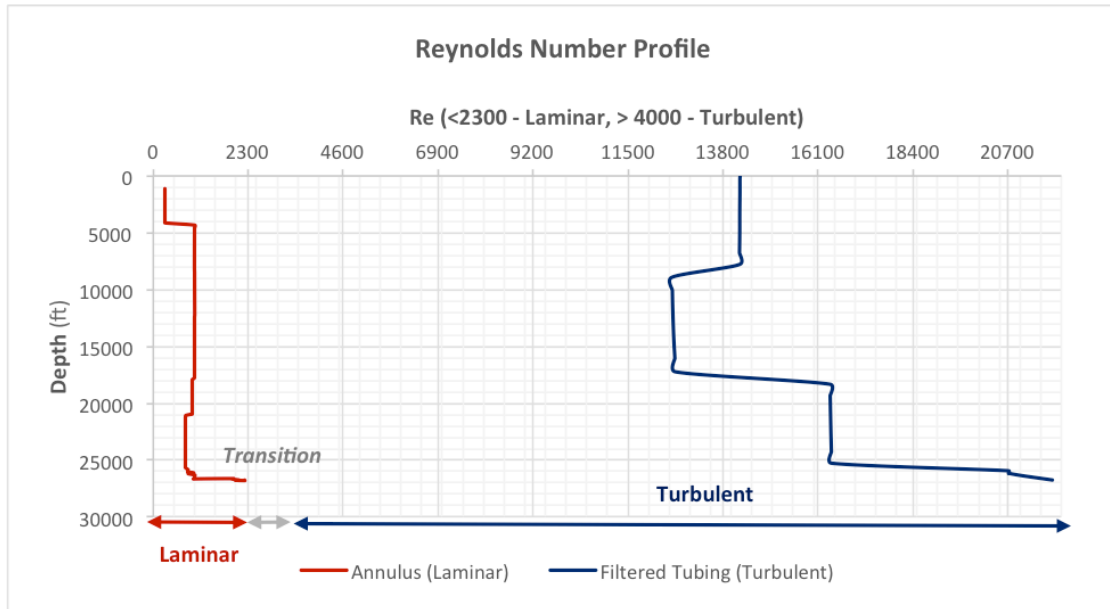


**Figure 47 - Reynolds Number Profile by Depth**

In **Figure 47**, we plot the Reynolds number profile with respect to depth of both the annulus and the drillstring. We note that the dominant flow regime for the annulus is laminar while the flow regime for the drillstring is turbulent. This makes physical sense as the laminar regime remains largely unchanged in diameter and pressure loss. In contrast, the BHA shown earlier has numerous diameters and pressure losses between string components along with the addition of an underreamer/hole opener.

We denote laminar below for a Reynolds number less than 2300 and turbulent for a Reynolds number exceeding 4000.

#### 4.18 Friction Pressure Loss Gradient

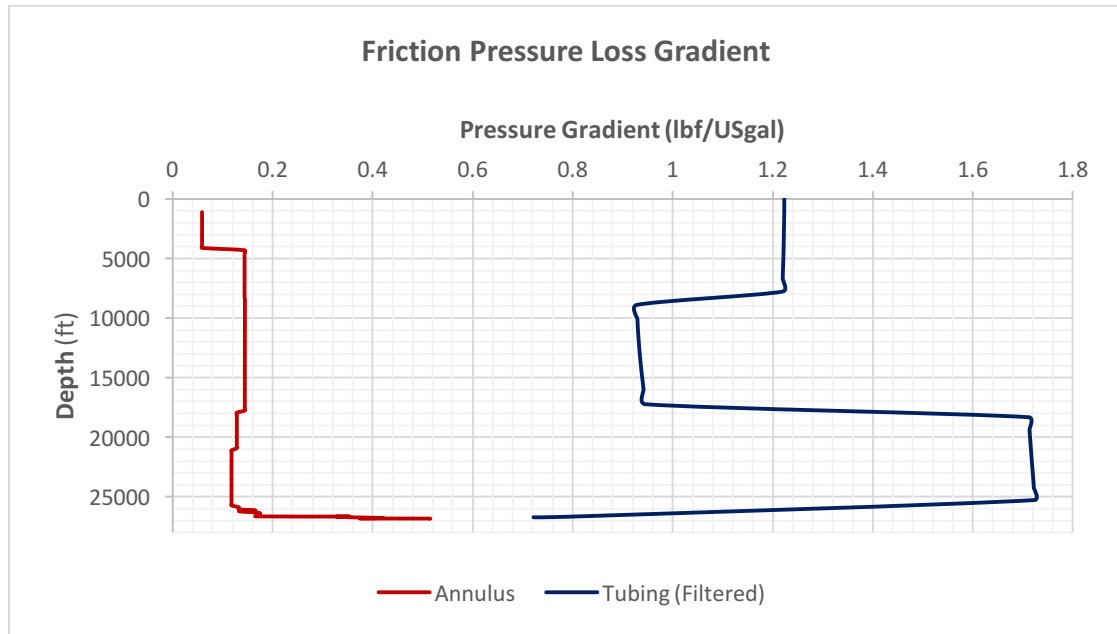


**Figure 48 - Frictional Pressure Loss Gradient by Depth**

We observe from **Figure 48**, the frictional pressure loss profile with respect to depth for both the drillstring and annulus. The separation or disconnect between the annulus and drillstring is due to the pressure loss of the bit, described in section 4.14. The annular pressure loss remains largely unchanged, as the flow regime itself is relatively static in the laminar phase. This differs greatly from the frictional pressure loss within the drillstring where there are numerous components with different inner

diameters, pressure losses, and additional equipment such as an underreamer/hole opener.

## 5. LIMITATIONS AND DEVELOPMENT

This research focuses on a specific given case and has limited flexibility in application to other wells. However, the fundamentals and simulation output is a solid reference for transient behavior in DGD. We discuss the limitations of both the software and the assumptions made throughout the duration of this research.

Drillbench is a robust software with respect to dynamic hydraulics; nevertheless, it has limitations in both scalability and functionality. We list some of the prominent differences between this simulation and actual transient behavior.

- EC-Drill's pump speed is controlled by an automatic pressure controller, which changes continuously, not in steps, as we presented.
- A PID controller then controls the subsea pump speed where gain and integral time are controller parameters. Drillbench lacks this functionality.
- Specific pump curves and head with respect to speed dictate flow through subsea pump. Drillbench lacks this specificity of input.
- Cuttings loading could contribute to a large increase in ECD. We neglected cutting in the simulation. We do however account for an increase in ECD in the drilling window.

Additionally, the software assumes two assumptions for the pressure calculation:

1. Fluids from the well into the DGD riser are normalized to standard conditions with respect to density (neglecting temperature)
2. Fluids are stacked according to density upon entrance of the riser with heavy density at the bottom in the discretization process

In terms of development and to address these limitations, DGD would have to be simulated in OLGA coupled with Drillbench for hydraulics and a functional programming language such as MATLAB for specific tasks. Irrespective of program or model, the following information would need to be obtained from industry:

1. Pore pressure and fracture pressure data
2. Downhole PWD data for statistical comparison
3. Pump head and speed curves
4. Temperature profile
5. Well trajectory if deviated
6. Lithology of well section

## 6. CONCLUSIONS

The primary objective of this research study was to investigate transient behavior during a drilling connection using software that could model hydraulics dynamically. As we explained in detail earlier, this research has application in addressing narrow pressure windows between pore pressure and fracture pressure.

This specific study aimed to highlight the efficacy of DGD in comparison to conventional drilling, specifically in addressing well control issues, U-tubing, and loss of annular frictional pressure loss. We remain positive that EC-Drill will provide innovative solutions to current deep-water challenges, especially to conventional wells once considered 'un-drillable'. We had the following criteria and constraints with respect to simulation design:

- 12.25" bit with 14.75" hole opener
- 4200' water depth with 19.5" ID riser
- ESD with full riser: 14.45 ppg
- Maximum ECD with cuttings: 14.90 ppg
- Mud: SOBM with MW 14.45 ppg, PV 22 cP, YP 17 lb/100ft<sup>2</sup>.
- Flow rate: 750 GPM
- Tolerance of BHP: +/- 75 psi

This specific study met all guidelines and constraints and was performed within reasonable computational cost and time with a high degree of accuracy. As mentioned earlier, the simulation software has the capability of reproducing field trials with accuracy in comparison to alternative steady-state competitors. However, the

simulation software lacks the scalability and functionality to model higher-complexity wells, for example, configurations with top fill and boost lines, control systems, etc.

## NOMENCLATURE

$A$	Area, ft <sup>2</sup> or m <sup>2</sup>
AFP	Annular Frictional Pressure Loss (psi)
Azi	Azimuth (degrees)
Bbls	Barrels
BHA	Bottomhole Assembly
BHP	Bottomhole Pressure (psi)
BML	Below Mud Line (ft)
CBP	Controlled Bottomhole Pressure (psi)
CML	Controlled Mud Level
$C_p$	Centipoise
$D$	Diameter (inches)
DGD	Dual Gradient Drilling
ECD	Equivalent Circulating Density
ESD	Equivalent Static Density
$f$	Friction Factor
FG	Fracture Gradient (pounds per gallon)
$f_{spm}$	Pump Pressure Head for Subsea Pump Module
GoM	Gulf of Mexico
GPM	Gallons Per Minute
$H_{max}$	Maximum Horizontal Stress
$H_{min}$	Minimum Horizontal Stress

hp	Horsepower
ID	Inner Diameter
Inc	Inclination (degrees)
KE	Kinetic Energy
MD	Measured Depth
ML	Mudline
MLP	Mudline Pump
MPD	Managed Pressure Drilling
MRL	Mud Return Line
MW	Mud Weight (pounds per gallon)
NCS	Norwegian Continental Shelf
$N_n$	Shaft Speed (rotations per minute)
NPT	Non-Productive Time
ROP	Rate of Penetration (ft)
$N_{Re}$	Reynold's Number
OD	Outer Diameter (inches)
P	Pressure
Psi	Pounds Per Square Inch
PE	Potential Energy
PP	Pore Pressure
PPG	Pounds Per Gallon
PV	Plastic Viscosity
$Q_n$	Volumetric Flow Rate

$Q_n$	Volumetric Flow Rate
RCD	Rotating Control Diverter
RKB	Rotary Kelly Bushing
RMR	Riserless Mud Return
ROP	Rate of Penetration
SICP	Shut-in Casing Pressure
SIDP	Shut-in Drilling Pressure
SMD	Subsea Mud-lift Drilling
SOBM	Synthetic Oil Based Mud
SPM	Subsea Pump Module
TD	Total Depth
TVD	Total Vertical Depth
$V$	Fluid Velocity
WD	Water Depth
YP	Yield Point
$\Delta L$	Unit Length
$\Delta P_n$	Pressure Loss
$\eta$	Pump Efficiency
$\rho$	Density
$\sigma$	Stress
$\omega_{spm}$	Pump Speed Measured in RPM

## REFERENCES

- Andriessse, D. (1976, January 1). Effect of Abnormal Pore Pressure on Deep Water Drilling. Society of Petroleum Engineers.
- Axon Energy Products. (2015, December). "Navigating Narrow Drilling Margins." *Drilling Pressure Control*. Web.
- British Geological Survey (BGS), n.d. "Borehole Breakout." *Rock Stress*. Web.
- Cohen, J. H., Stave, R., Hauge, E., & Molde, D. O. (2015, April 13). Field Trial of Well Control Solutions with a Dual Gradient Drilling System. Society of Petroleum Engineers.
- Cohen, John. (2014, September 12). "Two Gradients Are Better than One – Dual-gradient Drilling." *Drilling Features*. World Expro. Web.
- Drilling Handbook. (2015). "Well Control." *Kick Behavior*. Web.
- Enhanced Drilling, n.d. *EC-Drill® Managed Pressure Drilling System*. Web.
- Enhanced Drilling, n.d. "The Easier Approach To MPD." *EC Drill System*. Web.
- Georgia State University. (2010, January). "Pressure Physics." *Hyperphysics*. Web.
- Milnes, Matthew, n.d. "Mathematics of Pumping Water." *AECOM Design Build*. The Royal Academy of Engineering.
- Mirrajabi, M., Toftevag, K.-R., Stave, R., & Ziegler, R. F. (2012, January 1). First Application of EC-Drill in Ultra Deepwater: Proven Subsea Managed Pressure Drilling Method. Society of Petroleum Engineers.
- Mitchell, Robert F., Stefan Miska, and Bernt Sigve Aadnøy. (2011). *Fundamentals of Drilling Engineering*. Richardson, TX: Society of Petroleum Engineers. Print.
- Rehm, Bill, and Jerome Schubert. (2008). *Managed Pressure Drilling*. Houston, TX: Gulf Pub., Print.
- Rocha, L. A. S., Falcão, J. L., Gonçalves, C. J. C., Toledo, C., Lobato, K., Leal, S., & Lobato, H. (2004, January 1). Fracture Pressure Gradient in Deepwater.

Schubert, J. J., Juvkam-Wold, H. C., & Choe, J. (2006, December 1). Well Control Procedures for Dual Gradient Drilling as Compared to Conventional Riser Drilling.

Stave, R. (2014, May 5). Implementation of Dual Gradient Drilling. Offshore Technology Conference.

Vieira, P., Arnone, M. A., Cook, I., Moyse, K., Haojie, H. W., Qutob, H. H., ... Qing, C. (2008, January 1). Constant Bottomhole Pressure: Managed-Pressure Drilling Technique Applied in an Exploratory Well in Saudi Arabia. Society of Petroleum Engineers.

## SUPPLEMENTAL SOURCES CONSULTED

Gala, D. M., & Toralde, J. S. (2011, February 1). Managed Pressure Drilling 101: Moving Beyond "It's Always Been Done That Way." Society of Petroleum Engineers.

Godhavn, J.-M., Gaassand, S., Hansen, K. H., Morris, R., & Nott, D. (2015, April 13). Development and First Use of Controlled Mud Level System in US Deepwater GoM. Society of Petroleum Engineers.

Hauge, E., Godhavn, J. M., Molde, D. O., Cohen, J., Stave, R. S., & Toftevaag, K. R. (2015, May 4). Analysis of Field Trial Well Control Results with a Dual Gradient Drilling System. Offshore Technology Conference.

Jonggeun, C., Schubert, J. J., & Juvkam-Wold, H. C. (2004, January 1). Analyses and Procedures for Kick Detection in Subsea Mudlift Drilling. Society of Petroleum Engineers.

Skelton, J., Hogg, T. W., Cross, R., & Verheggen, L. (1995, January 1). Case History of Directional Drilling in the Cusiana Field in Colombia. Society of Petroleum Engineers.

Ziegler, R., Ashley, P., Malt, R. F., Stave, R., & Toftevag, K. R. (2013, April 17). Successful Application of Deepwater Dual Gradient Drilling. Society of Petroleum Engineers.

## APPENDIX A

### ADDITIONAL LITERATURE REVIEW

This overview will highlight key points on dual-gradient drilling methods with a focus on ‘controlled mud level drilling’ (CML). This additional literature review will comprise of five published papers and will present the results achieved by each well:

**Title:** Hauge, E., Godhavn, J. M., Molde, D. O., Cohen, J., Stave, R. S., & Toftevaag, K. R. (2015, May 4). **Analysis of Field Trial Well Control Results with a Dual Gradient Drilling System.** Offshore Technology Conference. doi:10.4043/26056-MS

#### **Problem**

*To analyze the results of a CMP field trial on three-laterals with a partly evacuated riser. Additionally, the paper attempts to quantify the ability to detect influxes and well control issues due to gas unloading.*

#### **Approach**

The field trial was performed on a drilling rig on the NCS. Five tests were conducted with a focus on both kick and loss detection and gas kick circulation with DGD. The five tests completed were:

- Liquid influx/loss detection
- Gas influx circulation
- Mitigation of gas flow in riser with top fill
- Gas influx detection
- Venting of gas into the riser

## **Conclusions**

The EC-Drill operator was able to detect volumes due to a sudden change in flow rate. However, the ability to detect influx/losses can be improved with finer tuning of the SPM PI-controller. Additionally, circulation of gas with a closed annular proved difficult to maintain a constant SPP while simultaneously encountering an increasing influx of gas. It is noteworthy to mention that a properly tuned PI-controller would most likely reduce the variations in the SPP.

## **Limitations**

The tests conducted were with completion mud and not drilling mud, and therefore results could be different. Also, a large gas-unloading event occurred due to high mud pump rate and large injection of gas. If flow rate was lower, it is more likely that gas would have been distributed more throughout the riser and would result in lower volumes of gas venting into the partially evacuated riser.

**Title:** Godhavn, J.-M., Gaassand, S., Hansen, K. H., Morris, R., & Nott, D. (2015, April 13).

**Development and First Use of Controlled Mud Level System in US Deepwater**

**GoM.** Society of Petroleum Engineers. doi:10.2118/173814-MS

**Problem**

*Analysis of rig modifications, training, success criteria, and results from first use of CML in US Deep-water GoM. Additionally, the paper will discuss Statoil's MPD solution for deep-water wells with collaboration with Maersk Drilling.*

**Approach**

The authors first define the two levels of CML operations:

1. CML-O –the riser level always maintains hydrostatic overbalance
2. CML-U –the riser fluid level may not provide hydrostatic overbalance

Additionally, Statoil followed the design acceptance criteria below in the development and test phase:

- Control riser pressure within 75 psi window
- Able to detect kick early
- Can operate conventionally in well-control
- Mitigation for gas in riser
- Verify ECD table calculations
- Stable riser level control

The EC-Drill SPM is run with the riser where the BOP and LMRP are picked up and the modified riser joint (MRJ) and SPM are installed. Once installed and system function are operational, tuning of the SPM pressure and flow controllers are necessary. The authors note that detecting a kick in transient situations such as a connection are more

difficult and therefore if each connection is done in the exact same manner, we can compare all future connections and riser pressure to the established baseline.

### **Conclusions**

More than 10,000 feet were drilled with a reduced riser level with approximately 600 pumping hours with no NPT. From this first deployment, Statoil and Enhanced Drilling have improved kick detection capabilities. The system provides two indicators for early kick detection –riser pressure and subsea pump speed.

### **Lessons Learned**

- Kick detection with low flow rate is still best seen on the active pit volumes
- EC-Drill technology with the adaptation of mud pump ramping and a quick closing annular will allow more accurate pressure control with respect to wellbore instability.
- The EC-Drill module can be used to confirm drilling margins and control losses by adjusting the riser fluid level.

**Title:** Mirrajabi, M., Toftevag, K.-R., Stave, R., & Ziegler, R. F. (2012, January 1). First **Application of EC-Drill in Ultra Deepwater: Proven Subsea Managed Pressure Drilling Method.** Society of Petroleum Engineers. doi:10.2118/151100-MS

### **Problem**

*A previous exploration well did not reach its objective due to the inability to maintain a WBM that was able to maintain circulation and not encounter losses. A system was sought out that allows adjustment of ECD dynamically.*

### **Approach**

The primary well objective was to reach a TD of 15,847 ft TVD in the carbonate reservoir where the EC-Drill system would be considered for drilling 2,067 ft of the 8 ½ hole section. The 8 ½” hole section was planned to be drilled with 8.8 ppg polymer WBM.

The maximum ECD reduction (MECDR) was calculated from the frictional pressure loss and effect of cuttings loading at the TD of the section. Through hydraulics modeling, the authors determined that the circulation pressure loss and cuttings loading will result in an increase in the BHP of a maximum of +/- 250 psi –equivalent to 547 feet of 8.8 ppg mud column.

Therefore, the approach was to ultimately reduce the BHP at TD by 547 feet of 8.8 ppg mud or 250 psi. The operators concluded that this window was well inside the EC-Drill operational window.

The riser pressure is continuously monitored and if a difference is detected between the riser pressure set-point and instantaneous riser pressure, the control system will adjust the subsea pump speed accordingly to reach the riser pressure set-point that was originally established.

### **Conclusions**

The authors note that conventional MPD procedures using an RCD would encounter difficulty in wellbore control with the closure of the annulus while under heave motion. It was concluded that the rig heave did not have a significant effect on control of BHP. The operator additionally observed that the wellbore pressure control was beneficial to minimizing costs, NPTs and the risks of kicks and losses. Most importantly, results show that EC-Drill minimizes formation/reservoir damage in the pay-zone areas.

### **Limitations**

The authors note that due to delays, the 8 ½" hole section has not been drilled yet and therefore the operational data for this specific hole section is not available. Additionally, due to the implementation of new technology, extensive training for the crew as well as utilizing a proprietary rig simulator software developed by AGR. Lastly, it is important to note that the three-stage subsea pump module can handle cuttings and gas cut mud up to 10%.

**Title:** Malt, R., & Stave, R. (2014, March 25). **EC-Drill MPD Dual Gradient Drilling for Challenging Pressure Regimes.** Offshore Technology Conference.

doi:10.4043/25455-MS

### **Problem**

*Current MPD systems with RCD employ low density mud weight and backpressure to achieve constant BHP. However, due to increasingly more complex and deeper wells, the authors from AGR Enhanced Drilling highlight that the EC-Drill technology is a valuable tool in preserving the integrity of the well.*

### **Approach**

The authors describe the general EC-Drill setup where the system is comprised:

- Subsea Pump Module (SPM) with 3 electrical pumps
- SPM is connected to a modified riser joint where the return line is a separate mud return line
- An umbilical line powers the SPM as well as handles communication from the SPM to the surface control system.

Additionally, the authors highlight the overall effect on well pressure when utilizing the EC-Drill. Traditionally, MPD systems use a lower MW than conventionally required and offset the difference by adding backpressure through the choke.

Increasing or decreasing the backpressure then adjusts BHP. This differs from the EC-Drill technology where the MW used is over-balanced and the riser level is reduced accordingly to achieve the desired BHP. The authors note the example calculation for the available pressure reduction window.

If the SPM is located 380 m below the RKB with a MW of 1.8 sg, the available pressure reduction is:

$$\text{Available Pressure} = 1.8 \text{ s. g.} \times 380 \text{ m} \times 0.0981 = 67.1 \text{ bar or } 973 \text{ psi}$$

Therefore, if the required ECD drop is needed to be 30 bar, there is an additional 37.1 bar that is available.

Additionally, the EC-Drill system was implemented successfully on 3 ultra-deepwater wells in the Caribbean. The objective was to adjust the BHP inside a window of 600 psi by adjusting the riser fluid level. Circulation rates were kept at 1600-1650 gpm for the first half of the 17.5" hole section and then later reduced to 1200-1300 gpm till the end.

### **Conclusion**

Using the riser level to adjust the wellbore pressure during drilling allows over-balanced MW at higher flow rates, while maintaining stability in the narrow pore-pressure/fracture-pressure gradient. Lastly, this system is valuable in its ability to cement weak formations with full returns and without losses.

**Title:** Ziegler, R., Ashley, P., Malt, R. F., Stave, R., & Toftevag, K. R. (2013, April 17).

**Successful Application of Deepwater Dual Gradient Drilling.** Society of Petroleum Engineers. doi:10.2118/164561-MS

### **Problem**

*The authors present the technology applied, specifically EC-Drill, while analyzing the results achieved in drilling a well with 2260m water depth. Whilst drilling, the rig encountered gas bearing formations with a reduced riser level – however, no gas was seen at the riser surface.*

### **Approach**

The objectives for well C-1 using the EC-Drill system were as follows:

- Assist operator in drilling to planned TD without losses or wellbore instability
- Provide evidence that ECD can be reduced/eliminated in ALL sections of the well
- Provide good hole cleaning in all sections
- Increase the ROP (comparison to offset)
- Prove that in a partially evacuated riser that gas is not a problem with reduced riser level

Pre-drilling tests were completed by performing a functional test that included verifying all valves and system controls were operating correctly. Secondly, they tested the EC-Drill to 90% capacity as well as adjusting fluid level while stopping pumps for a connection. Finally, the PID controller was fine-tuned while lowering the riser level.

For each trip, both sections had the riser filled before any tripping occurred. At this point, the EC-Drill is isolated and conventional tripping commences. The operators note that the ability to trip DP with adjustable riser level is advantageous over the often-used MPD with RCD systems.

During drilling, the ECD was measured using the PWD sensor on the downhole tool – where it confirmed that at all times, the wellbore pressure was overbalanced to the pore pressure. Any kick/losses that occur with DGD are treated on-the-fly by adjusting the riser fluid level rather than shutting in the BOP. This is also advantageous to conventional well control where the formation may not allow circulation through the choke/kill line as noted by the authors.

### **Conclusions**

1. The EC-Drill system was dynamically able to adjust a riser level of 150-200 m with a flow rate of 1650 gpm.
2. No losses or influxes were seen or detected throughout all sections
3. ROP increased with decreases in BHP
4. No gas was detected in the partially evacuated riser at surface.

## APPENDIX B

### BOTTOMHOLE ASSEMBLY

Attached on the next page is the complete specification sheet for the BHA and drillstring in **Table 5**. The following information is summarized on **Table 2, 3, and 4** below:

1. Sensor offsets from bit
2. Stabilizer summary
3. BHA Nozzle Summary

**Table 2 - Sensor Offset From Bit (Statoil ASA)**

<b>Sensor Offset from Bit (ft)</b>	
Gamma Ray	7.56
D+I	8.36
APWD	26.46
ARC Resistivity	28.79
ARC Gamma Ray	28.96
D+I	56.74
FPWD	79.17
Sonic	126.22
Density	149.88
Neutron	156.39

**Table 3 - Stabilizer Summary (Statoil ASA)**

<b>Stabilizer Summary</b>		
Blade Mid-Pt to Bit (ft)	Blade OD (in)	Blade Length (ft)
17.725	12.125	1.270
41.880	12.125	1.500
75.320	12.000	2.280
112.000	12.000	0.525
132.640	12.000	0.525
149.170	12.000	3.580
157.250	11.650	3.258
180.640	12.125	2.200
189.165	11.500	4.583
234.290	12.250	2.100

**Table 4 - BHA Nozzle Summary (Statoil ASA)**

<b>BHA Nozzle Summary</b>			
Bit Nozzle		Reamer Nozzle	
Count	ID (1/32 in)	Count	ID (1/32 in)
6	14.000	1	8.000
1	15.000		
TFA (in2)	1.075	TFA (in2)	0.049

**Table 5 - BHA Specification Sheet (Statoil ASA)**

	Desc.	Manu.	OD (in)	Max OD (in)	Bot Size (in)	Bot Type	Bot Gender	FN OD (in)	Length (ft)	Cum. Length (ft)	Cum. Weight (1000 lbm)
			ID (in)		Top Size (in)	Top Type	Top Gender	FN Length (ft)			
1	12 1/4" PDC Bit	Smith	8.000	12.250					0.96	0.96	0.4
			3.000		6.625	Regular	Pin				
2	PD900 X5 12 1/4" Slick CC	Schlumberger	9.000	11.960	6.625	REG	Box		13.45	14.41	2.8
			5.125		6.625	REG	Box				
3	12 1/8" NM Receiver Stabilizer	Schlumberger	8.375	12.125	6.625	Regular	Pin	8.375	6.02	20.43	3.9
			3.500		6.625	FH	Box	1.90			
4	arcVISION825(GR-RES-APWD)	Schlumberger	8.375	9.125	6.625	FH	Pin	8.375	19.45	39.88	7.0
			4.250		6.625	FH	Box	4.76			
5	Telescope 825 w/bttm 12 1/8 Sleeve Stab (Survey/IWOB/MVC)	Schlumberger	8.625	12.125	6.625	FH	Pin	8.375	30.65	70.53	11.4
			4.250		6.625	FH	Box	1.37			
6	StethoScope 825 w/ 12" Stabilizer	Schlumberger	8.250	12.000	6.625	FH	Pin	8.250	36.00	106.53	16.4
			5.900		6.625	FH	Box	1.03			
7	SonicScope 825 w/ (2) 12"Stabilizers	Schlumberger	8.250	12.000	6.625	FH	Pin	8.375	32.70	139.23	20.7
			5.807		6.625	FH	Box	4.51			
8	SADN8 (DEN-NEU) w/ (2) 12" Stabilizers	Schlumberger	8.250	12.000	6.625	FH	Pin	8.000	29.40	168.63	24.2
			3.250		6.625	Regular	Box	6.71			

**Table 5 - Continued**

	Desc.	Manu.	OD (in)	Max OD (in)	Bot Size (in)	Bot Type	Bot Gender	FN OD (in)	Length (ft)	Cum. Length (ft)	Cum. Weight (1000)
9	NM Downhole Filter Sub	Mashburn	8.063	8.063	6.625	Regular	Pin		7.55	176.18	25.3
			3.063		6.625	Regular	Box				
10	12 1/8" NM IB Stabilizer w/ non-ported (Auto Fill) float valve	StabilDrill	8.250	12.125	6.625	Regular	Pin	8.313	6.34	182.52	26.3
			3.063		6.625	Regular	Box	2.96			
11	12 1/4 x 14-3/4" RhinoXS Reamer 11625 Series w/ non-ported (Auto-Fill) float valve (TFA: 0.049,1x8)	Smith	8.160	11.500	6.625	Regular	Pin	8.250	16.88	199.40	30.0
			3.000		6.625	Regular	Box	4.90			
12	1 x 8 1/4" Spiral Drill Collar	Rig	8.250	8.250	6.625	Regular	Pin	8.250	31.04	230.44	34.8
			2.813		6.625	Regular	Box	1.35			
13	12 1/8" NM IB Stabilizer	StabilDrill	8.250	12.250	6.625	Regular	Pin	8.250	8.07	238.51	36.1
			2.875		6.625	Regular	Box	3.17			
14	11 x 8 1/4" Spiral Drill Collars (11 joints)	Rig	8.250	8.250	6.625	Regular	Pin	8.250	336.82	575.33	87.9
			2.813		6.625	Regular	Box	1.09			
15	Crossover	Quail	8.500	8.500	6.625	Regular	Pin		4.43	579.76	88.7
			3.063		6.625	FH	Box				
16	3 x 6 5/8" HWDP (3 joints)	Quail	6.625	8.500	6.625	FH	Pin	8.500	91.52	671.28	96.0
			4.500		6.625	FH	Box	1.50			
17	Hydra-Jar 8"	Schlumberger	8.000	8.160	6.625	FH	Pin	6.500	33.01	704.29	99.6
			3.000		6.625	FH	Box	2.48			

**Table 5 - Continued**

	<b>Desc.</b>	<b>Manu.</b>	<b>OD (in)</b>	<b>Max OD (in)</b>	<b>Bot Size (in)</b>	<b>Bot Type</b>	<b>Bot Gender</b>	<b>FN OD (in)</b>	<b>Length (ft)</b>	<b>Cum. Length (ft)</b>	<b>Cum. Weight (1000 lbm)</b>
18	11 x 6 5/8" HWDP (11 joints)	Rig	6.625	8.250	6.625	FH	Pin	8.500	337.67	1041.96	126.4
			4.500		6.625	FH	Box	1.50			
19	Crossover	Rig	8.375	8.375	6.625	FH	Pin	7.000	4.26	1046.22	127.1
			3.000		5.875	VX57	Box	2.01			
20	5-7/8 " 26.30 (0.415wt) DPS, 10% Wear (180 joints)	Rig	5.792	7.000	5.875	VX57	Pin		7936.58	8982.80	359.3
			5.045		5.875	VX57	Box				
21	Crossover	Rig	7.000	8.250	5.875	VX57	Pin		3.42	8986.22	359.6
			4.250		6.625	VX65	Box				
22	6-5/8 " 31.20 (0.475wt) DPS, 10% Wear (216 joints)	Rig	6.530	8.250	6.625	VX65	Pin		9519.18	18505.40	702.9
			5.675		6.625	VX65	Box				
23	Crossover	Quail	8.500	8.500	6.625	VX65	Pin		3.15	18508.55	703.4
			3.000		6.625	FH	Box				
24	6-5/8 " 40.00 (0.625wt) DPZ, 10% Wear to Surface (210 joints)	Quail	6.500	8.500	6.625	FH	Pin		9170.39	27678.94	1151.6
			5.375		6.625	FH	Box				